



Doxorubicin loaded octacalcium phosphate particles as controlled release drug delivery systems: Physico-chemical characterization, *in vitro* drug release and evaluation of cell death pathway

Ilijana Kovrlija^{a,b}, Elżbieta Pańczyszyn^{c,1}, Ozgur Demir^{a,b,1}, Marta Laizane^{a,b}, Marco Corazzari^{c,d}, Janis Locs^{a,b}, Dagnija Loca^{a,b,*}

^a Institute of Biomaterials and Bioengineering, Faculty of Natural Sciences and Technology, Riga Technical University, Pulka 3, Riga LV-1007, Latvia

^b Baltic Biomaterials Centre of Excellence, Headquarters at Riga Technical University, Riga, Latvia

^c Department of Health Science & Center for Translational Research on Autoimmune and Allergic Disease (CAAD), University of Piemonte Orientale, 28100 Novara, Italy

^d Interdisciplinary Research Center of Autoimmune Diseases (IRCAD), University of Piemonte Orientale, Novara, Italy

ARTICLE INFO

Keywords:

Octacalcium phosphate
Doxorubicin
Drug delivery
Apoptosis
Osteosarcoma cells
MC3T3-E1

ABSTRACT

Mastering new and efficient ways to obtain successful drug delivery systems (DDS) with controlled release became a paramount quest in the scientific community. Increase of malignant bone tumors and the necessity to optimize an approach of localized drug delivery require research to be even more intensified. Octacalcium phosphate (OCP), with a number of advantages over current counterparts is extensively used in bone engineering. The aim of the present research was to synthesize bioactive and biocompatible doxorubicin (DOX) containing OCP particles. DOX-OCP was successfully obtained *in situ* in an exhaustive range of added drug (1–20 wt%, theoretical loading). Based on XRD, above 10 wt% of DOX, OCP formation was inhibited and the obtained product was low crystalline α -TCP. *In-vitro* drug release was performed in pH 7.4 and 6.0. In both pH environments DOX had a continuous release over six weeks. However, the initial drug burst for pH 7.4, in the first 24 h, ranged from 15.9 ± 1.3 % to 33.5 ± 12 % and for pH 6.0 23.7 ± 1.5 % to 36.2 ± 12 %. The DOX-OCP exhibited an inhibitory effect on viability of osteosarcoma cell lines MG63, U2OS and HOS. In contrast, MC3T3-E1 cells ($IC_{50} > 0.062$ μ M) displayed increased viability and proliferation from 3rd to 7th day. Testing of the DDS on ferroptotic markers (CHAC1, ACSL4 and PTGS2) showed that OCP-DOX does not induce ferroptotic cell death. Moreover, the evaluation of protein levels of cleaved PARP, by western blotting analysis, corroborated that apoptosis is the main pathway of programmed cell death in osteosarcoma cells induced by DOX-OCP.

1. Introduction

One of the frontline difficulties of today's society is a myriad of different types of cancer. It has been projected that by the onset of 2040, global cancer cases will reach staggering 26 million, with 15 million people standing in need of chemotherapy (Wilson et al., 2019). According to the publicly available data, bone tumours comprise roughly 3–5 % of juvenile cancers and less than 1 % of cancers in adults. Osteosarcoma (OS) is one of the main representatives of malignant skeletal tumour (accounting to ~ 40 % of bone tumours), most commonly diagnosed as the primary malignant bone tumour. Treatment of OS is essentially based on various chemotherapies, followed by surgical

resection, while only a scarce number of alternatives are present (vaccines, immune checkpoint inhibitors, monoclonal antibodies) (Martinez et al., 2021). Even though chemotherapy is extremely important as adjuvant therapy, significant data suggests that osteoporosis is an unwanted side effect, resulted from accelerated loss of bone mineral density due to the treatment (Guise, 2006; Siebler et al., 2002). Recent study has demonstrated that senescence (loss of a cell's power of division and growth) propels age-related bone loss contributing to an already dangerous chemotherapy-induced bone loss (Yao et al., 2020).

Doxorubicin hydrochloride (DOX, Doxorubicin, Adriamycin) is a photosensitive, water-soluble chemotherapeutic drug, derived from *Streptomyces peucetius* var. *caesius*. It is being extensively used as the

* Corresponding author at: Institute of Biomaterials and Bioengineering, Riga Technical University, Pulka Street 3, LV-1007, Riga, Latvia.

E-mail address: dagnija.loca@rtu.lv (D. Loca).

¹ Equal input from both Authors.

first-line therapy for a variety of cancers, among which are osteogenic bone cancers (Sritharan & Sivalingam, 2021). Even though DOX has a reputation as a well-established and highly effective anti-neoplastic agent (Sritharan & Sivalingam, 2021; Tacar et al., 2012; van der Zanden et al., 2021), the successful use of it has been hampered by toxicities ranging from nausea and hematopoietic suppression, to an increased risk of doxorubicin-induced cardiomyopathy (Olson & Mushlin, 1990; van der Zanden et al., 2021; Yin et al., 2018). DOX toxicity is connected with intravenous administration of the drug and its initial half-life of eight minutes and a terminal half-life of 30 h (40 % of the administered dosage gets metabolized by other organs) (Sritharan & Sivalingam, 2021). This initial drug burst (large amounts of the drug are being released before the release rate reaches a stable profile) can have a less negative effect if the delivery of DOX is targeted. Research has shown that the lower initial burst and slower *in vitro* release of doxorubicin loaded microparticles resulted in a lower short term cytotoxicity to Glioma C6 cells when compared to the free drug (Lin et al., 2005). Additional hindrance to the treatment of OS is chemoresistance, usually triggered by the cells poor reaction to the initial therapy or the acquired resistance developed over time. Chemoresistance of osteosarcoma cells to DOX is found to be coupled with the increased drug efflux via p-glycoprotein, mutations in topoisomerase II enzyme, DNA damage repair and surge of detoxification. To increase its widespread applicability and to limit the development of chemoresistance and dosage-dependent toxicity, it is of paramount importance to design a drug delivery system (DDS) that will regulate the localized administration and short/long-term effects of doxorubicin. For that reason, several research groups have investigated the combination of DOX with nanoparticles, liposomal formulations or polymers (Elbayoumi & Torchilin, 2009; Gautier et al., 2012; Modh et al., 2021; A. Z. Wang et al., 2012). Following these benchmarks, calcium phosphates (CaPs), functionalized with drugs/ions for biological or therapeutical applications, have been occupying the scientific headlines in the field of bone therapy (Lebugle et al., 2002; Loca et al., 2015; Mosina et al., 2022).

One of the most important members of CaPs, octacalcium phosphate (OCP, $\text{Ca}_8(\text{HPO}_4)_2(\text{PO}_4)_4 \times 5\text{H}_2\text{O}$), has been postulated to be a precursor of biological apatite crystals due to its intrinsic structure (Kovrljija et al., 2021; L.C.Chow & Eanes, 2001; Mathew et al., 1988). Next to the abundant accounts of OCP enhancing the bone formation (Anada et al., 2008; Saito et al., 2021; Suzuki & Insley, 2020), as of recently it is being reported as a potent drug delivery vehicle for the incorporation of different therapeutical agents (Kovrljija et al., 2021). OCP has several advantages over other calcium phosphates in terms of a possible drug carrier. The peculiar arrangement of the structure, crystallographic planes resembling the ones from apatite, and a relatively empty water layer (approximately 0.8 nm in thickness), enables the incorporation of distinct ions and molecules inside and not only by adsorption (L.C.Chow & Eanes, 2001). OCP has the ability to readily convert to a thermodynamically more stable phase, calcium deficient hydroxyapatite (CDHAp), demonstrating an ameliorated effect on the bone formation (Honda et al., 2007). Furthermore, the fact that it has higher solubility than the stoichiometric hydroxyapatite (0.0081 g/L at 25 °C for OCP, and 0.0003 g/L for HAp) can directly influence the drug release kinetics and the overall release profile (Dorozhkin, 2016). With this OCP has the potential of a triple effect on sustained delivery of DOX: initial burst release from the DOX molecules adsorbed on the surface of OCP, release of DOX incorporated inside of the OCP's water layer caused by the gradual transformation to apatite and if OCP was combined with a polymer (e.g. alginate) it would allow an even more prolonged drug release as the construct would degrade. As envisioned DDS would be implemented locally in the tumour site and the form of the end application can vary. OCP has been used as a composite coating on titanium alloys (Bordbar-Khiabani et al., 2023), as an injectable cement paste (Demir et al., 2023) or in the form of pellets (Lebugle et al., 2002). Together with the local distribution of the drug, such OCP construct could later on mimic the formation of biomimetic apatite and boost the

healing and regeneration processes.

As a drug delivery system, OCP has been previously used in the cancer research and it showed promising results. Main findings have focused on the combined effect with an antineoplastic agent, methotrexate (MTX). Lebugle et al. (Lebugle et al., 2002) have used implants, made mostly from partly hydrolysed OCP and dextran, which were doped with 2, 4 and 6 % of MTX and subsequently tested for *in vitro* and *in vivo* pharmacokinetics and biocompatibility. *In vitro* release profile resulted in 95.2 %, 68.3 % and 71.9 % of released MTX for granules containing 2 %, 4 % or 6 % of drug, respectively. In *in vivo* environment, 75 % of 2 % MTX remained in the doped implants after 24 h, and 25 % after a week. Ito's research group (Ito et al., 2014), observed the behaviour of a mixture of OCP and HAp as a new potential drug carrier for MTX. Here, the specific characteristic of OCP to hydrolyse into CDHAp were postulated to be the assisting mechanism of the drug release. Tested DDS was capable of retaining the drug, while the release profile was continuous for 48 h and the proliferation of human osteosarcoma cell line was considerably inhibited (1×10^5 cells, while the control had 4×10^5 cells, approximately). Another interesting approach was the functionalization of OCP with extrinsic iron ions and their combination into a scaffold with poly(lactic-co-glycolic acid) for chemotherapy and bone repair after surgery (Shi et al., 2019). Presented DDS sustained human umbilical vein endothelial cell (HUVECs) adhesion and spreading *in vitro* and prompted improved angiogenesis *in vivo*. Model proteins (bovine serum albumin and lysozyme) were significantly greater than on the control without doping (~8.5 and 9.5 mg/g, respectively), neovascularization was higher (after 4 weeks implantation from 71.7 ± 6.6 to 99.8 ± 9.8 per mm^2 , depending on the concentration of ion), and DDS had higher stimulatory effects on potential vascularization (~0.25 IOD/area).

Several inorganic CaP biomaterials have been combined with DOX. DOX-loaded apatite particles have shown the cytotoxic behaviour toward human SAOS-2 osteosarcoma cells *in vitro* (~0.2 absorbance, while control had ~0.6) (Iafisco et al., 2016). Furthermore, a self-setting paste – combining amorphous calcium phosphate and doxorubicin loaded particles of bone-like carbonated nanocrystalline apatite, have been tested and the *in vivo* implantation was carried out (Martinez et al., 2021). Average number of metastatic pits was 2.0 for the DDS, versus 3.3 for the control, which represented a decrease of nearly 40 %. DOX was also combined with nano and micro HAp by immersing them in dissolved DOX in phosphate-buffered saline (PBS) at different pH (Y. Liu et al., 2022b). At pH 2.5, 81 % DOX was released from nano HAp during 72 h. 46 % DOX was released at pH 5 and at pH 7.4 16 % of the drug was released. For the complex with micro HAp at pH 5.6–6.8, 8–16 % of the drug was released extracellularly compared to pH 7.4. Overall, in *in vivo* setting, micro HAp complex and nano HAp complex had the same antitumor efficacy, whereas micro HAp-DOX was less cytotoxic to MC3T3 cell line compared to nano HAp alone within the 50–100 µg/mL concentration range. When HAp was combined with alfa hemihydrate calcium sulfate (40 to 60 ratio), the biphasic material released 28 % DOX *in vitro* during the first week and at pH 5, 36 % was released, with a strong cytotoxic effect on both MG-63 cells (75 %) and 143B cells (98 %) (Y. Liu et al., 2021). The aforementioned combination of the anticancer drugs and different OCPs could also be the potential strategy to reduce presence of osteosarcoma drug-resistant phenotype, as well as to treat the disease after the therapeutic effect has gone (with the bone regenerative properties of CaPs) (Cree & Charlton, 2017; Nussinov et al., 2021; Pisa & Kapoor, 2020). Moreover, the usage of the local drug delivery systems eliminates the systemic toxicity and lowers the needed amount of the drug. However, to our knowledge, when it came to functionalizing OCP with doxorubicin, DDS that preserves the unique OCP phase and shows anti-osteosarcoma properties has not yet been developed.

Hence, in order to go one step further with the design of a suitable drug delivery vehicle for the bone cancers, a novel, *in situ* synthesis of doxorubicin doped octacalcium phosphate (DOX-OCP) via the

hydrolysis of α -tricalcium phosphate (α -TCP), has been performed. OCP has been functionalized with DOX in a large doping range (from 1 wt% to 20 wt% of theoretical DOX loading). Products were analyzed by an extensive multi-technique characterization approach with X-ray diffractometry (XRD), to certify the existence of OCP phase, and Fourier-transform infrared spectroscopy (FTIR) to show hydrogen phosphate ($\text{HPO}_4(5)$ and $\text{HPO}_4(6)$) group P-(OH) stretch and OH in-plane bend. Furthermore, scanning electron microscopy (SEM) was performed to show the morphology of the novel DDS. After establishing the physicochemical characteristics of the materials, the *in vitro* release kinetics of doxorubicin in phosphate-buffered saline (PBS) at pH 7.4 and pH 6.0 were assessed over a six-week period using ultraviolet-visible spectrometry (UV-Vis). Furthermore, as prepared local drug delivery systems (DOX-OCP) were subjected to the cytocompatibility evaluation with human osteosarcoma cell lines, MG-63 and murine calvarial cell line, MC3T3-E1. The cytotoxicity of the DOX towards MG63 and MC3T3-E1 cells was also assessed by determining the IC50 values. The choice of using both MG63 and MC3T3-E1 cell lines enables a comparative analysis of the response between cancer cells (MG63) and normal cells (MC3T3-E1), when exposed to the DOX-OCP drug delivery system. By studying the impact of DOX loaded OCP powders on MG63 cells, valuable insights can be gained regarding the development of effective *in vivo* drug delivery systems for bone cancer treatment (Banerjee & Bose, 2019). Additionally, assessing the effects on MC3T3-E1 cell line, provides important information on the system's efficacy in post-tumor excision treatments and its potential to reduce metastases (Pinski et al., 2001).

Apoptosis has long been considered a deliberate mechanism of programmed cell death (PCD) and the pathways involved in this process have been extensively studied in various types of tumour cells (X. Wang et al., 2022). Moreover, the induction of apoptosis was recognized as a prominent therapeutic approach for eliminating cancer cells (Ji et al., 2015; J. Li et al., 2016; Pfeiffer & Singh, 2018; Singh et al., 2022). However, recent increasing evidence has proven that an anti-tumour strategy based on the induction of non-apoptotic cell death is a promising direction for addressing certain challenges (e.g., poor chemotherapy efficacy, genomic alterations, low tumour cellularity) in the cancer therapy (X. Wang et al., 2022). Ferroptosis is a newly discovered form of PCD that differs from apoptosis, necrosis, and autophagy at both morphological and biochemical levels (Xuejun Jiang et al., 2021). Ferroptosis characteristics, identified by iron-dependent accumulation of lipid peroxides and inhibition of GPX4, highlight new treatment opportunities for cancers that are resistant to conventional therapies, including osteosarcoma (S. Li et al., 2023; X. Liu et al., 2022b; Qiu et al., 2022). Furthermore, the recently developed therapeutic agent for osteosarcoma by Fu et al., was observed to impede tumour growth through the induction and synergistic interaction of ferroptosis and apoptosis (Fu et al., 2021). Osteosarcoma exhibits high genetic heterogeneity, leading to variations in genomic and proteomic profiles among cell lines. Consequently, these cells may display diverse differentiation capacities, ranging from osteoblastic to other phenotypes resembling neoplasms *in vivo*. Moreover, differences in tumor formation capacity, influenced by the composition of the extracellular matrix (ECM), and metastatic potential, determined by the expression of specific markers, contribute to their aggressiveness. These variations can significantly impact tumor response to treatment and overall therapy outcomes. Hence, employing a variety of cell lines is essential when screening for PCD. Therefore, in order to test which pathway of cell death is undergoing when exposed to OCP-DOX DDS, we evaluated the induction and execution of both apoptosis and ferroptosis with a panel of OS cells – U2OS, MG63 and HOS.

Through this comprehensive evaluation, our study aims to enhance the understanding of the effects DOX-OCP drug delivery system has on bone cancer cells, leading to the development of improved treatment strategies to minimize metastasis after tumour excision. Furthermore, present research helps to understand the role OCP could have in the

incorporation of a known chemotherapeutic drug, and the synergy effects the presented construct could have on the biological response. This would provide a new, alternate, functionalized bone material for therapeutic applications.

2. Materials and methods

2.1. Materials

The following reagents have been used throughout the experiments: orthophosphoric acid (H_3PO_4 , 75 %) was purchased from Latvijas Ķīmija, Latvia. Doxorubicin hydrochloride (DOX, Lot 20120715) was purchased from CHEMOS GmbH Germany and from Merck, Milan, IT, hydrochloric acid (HCl, 37 %, Lot Z0720617 111) was purchased from Emsure®, Germany and phosphate buffered saline (PBS, Lot SLCH0989) from Sigma Aldrich, USA. Dulbecco's phosphate buffered saline (DPBS) was purchased from Sigma Aldrich (Darmstadt, Germany) and Gibco™ and Thermo Fisher, USA. Dimethyl sulfoxide (DMSO) was purchased from Sigma Aldrich, USA. 24-well plates with insert purchased from VWR, USA. Minimum essential medium α (MEM- α), penicillin-streptomycin (pen-strep), fetal bovine serum (FBS) and Trypsin EDTA 1X were acquired from Gibco™, Thermo Fisher, USA and from EuroClone, Pero, IT. MG63 and MC3T3-E1 cells (LOT:7009744) were purchased from ATCC, USA. Cell counting kit-8 (CCK-8) and CellTiter Blue assay kit were purchased from Sigma Aldrich, USA. U2OS, MG63 and HOS osteosarcoma cell lines (used to test cell death with 1DOX-OCP) were purchased from 'Biological Resource Center ICLC Cell bank, Core facility IRCCS Ospedale Policlinico San Martino, Genova (IT). Dulbecco's modified Eagle's medium – DMEM, EuroClone; Pero, IT. L-glutamine was from Sigma-Aldrich; Milan, IT and Ferrostatin-1 (Fer1) from Merck, Milan, IT. AlamarBlue™ reagent (Bio-Rad; Berkeley, CA, US) and multiwell inserts (0.4 μm pore size; Sarstedt, Germany). TripleXtractor reagent (Grisp; Porto, PT); ExcelRT™ Reverse Transcription Kit (SMOBIO, Bio-Cell; Rome, IT) and RIPA Buffer supplemented with a protease inhibitor cocktail (Merck, Milan, IT). Non-fat dry milk (Merck, Milan, IT), and Tween20 (Merck, Milan, IT). Primary antibodies: anti-cleaved PARP (1:1000, Cell Signaling Technology; Danvers, US); anti-Tubulin (1:1000, Santa Cruz Biotechnology, Dallas, US), secondary antibodies (1:5000; Bio-Rad) and SuperSignal West Pico Plus (ThermoFisher).

2.2. Synthesis methodology

2.2.1. Synthesis of octacalcium phosphate

To obtain α -TCP, amorphous calcium phosphate (ACP) was synthesized and heated for one hour at 650 °C (5 °C/min) (Kovrlija et al., 2023). Prior to OCP synthesis, α -TCP was fully analyzed and its phase composition was corroborated with XRD. 100 mg of α -TCP were immersed into 50 mL of 0.0016 M H_3PO_4 solution at room temperature, under unremitting stirring (300 rpm), during the 24 h period. pH was monitored throughout the entire time frame. Obtained sample was washed with deionized water and left to dry at 37 °C. The obtained octacalcium phosphate is further referred to as the OCP. The synthesis have been performed more than five times in order to claim the formation of OCP.

2.2.2. Incorporation of doxorubicin in octacalcium phosphate

Same procedure of α -TCP hydrolysis towards OCP was used for the drug incorporation. 100 mg of α -TCP and corresponding amount of theoretical DOX load (1, 3, 5, 7, 8, 9, 10 and 20 wt%) were simultaneously immersed into 50 mL of 0.0016 M H_3PO_4 solution at room temperature for 24 h, with constant stirring (300 rpm). Obtained samples were left to dry at 37 °C. The obtained doxorubicin loaded octacalcium phosphate is named depending on the theoretical loading amount of DOX that was added (see Table 1). Additional samples were synthesized in the same manner with 12, 15 and 18 wt% of DOX to

Table 1
Identification of obtained doxorubicin loaded calcium phosphates.

Sample name	Precursor	Theoretical amount of DOX used (wt%)
OCP	α -TCP	0
1DOX-OCP		1
3DOX-OCP		3
5DOX-OCP		5
7DOX-OCP		7
8DOX-OCP		8
9DOX-OCP		9
10DOX-OCP		10
12DOX-CaP		12
15DOX-CaP		15
18DOX-CaP		18
20DOX-CaP		20

ascertain the CaP phase that is being formed between the further tested 10 wt% and 20 wt% of DOX. However, they were not used in the *in vitro* drug release and cytotoxicity assessments. The synthesis have been performed more than five times in order to claim the formation or inhibition of OCP phase.

2.2.2.1. Assessment of doxorubicin adsorption on octacalcium phosphate.

In order to test whether the *in situ* methodology of adding doxorubicin to OCP results in the drug being incorporated into OCP, an adsorption test was carried out in the following manner. 100 mg of OCP and 9 mg of DOX (corresponding to the 9DOX-OCP from the *in situ* loading) were added in 50 mL of PBS and stirred continuously for 24 h (300 rpm). Obtained samples were left to dry at 37 °C. As obtained product (referred further as 9DOX-OCP ads.) was tested with XRD and subjected to *in vitro* drug release test for 48 h in PBS pH 7.4.

2.3. Phase and composition characterization

2.3.1. X-ray diffraction

Presence of OCP phase was examined by using X-ray powder diffractometry. XRD was completed using PANalytical Aeris diffractometer (The Netherlands) and complementary analysis were done with X'PertHighScore and the International Centre for Diffraction Data PDF-2 (ICDD) database. To obtain XRD pattern the following parameters were used: 40 kV and 15 mA, step size 0.0435°, from 3° to 60° 2 θ degrees and time per step 299.575 s. For crystalline phase identification ICDD entries were used – #026–1056 for OCP and #009–0348 for α -TCP.

2.3.2. Fourier-transform infrared spectroscopy

Fourier transform infrared spectrometer Thermo Scientific Nicolet™ iS™50 (Waltham, MA, USA), used in Attenuated Total Reflectance (ATR) mode, was employed to characterize functional groups of powders at the molecular level. The FTIR spectra were recorded in the range 4000–400 cm⁻¹, with the number of scans 64, at a resolution of 4 cm⁻¹. The processing software was OMNIC.

2.3.3. Scanning electron microscopy

The surface morphology of the OCP and DOX-OCP was visualized by scanning electron microscope (Tescan Mira\LMU, Tescan, Czech Republic). Sample image generation was performed with combination of secondary electrons and back-scattered electrons, created at an acceleration voltage of 5 kV. Samples were secured with an electrically conductive double-sided adhesive carbon tape, on a standard aluminium pin stubs. Prior to the SEM measurement, samples were sputter coated with gold, using Emitech K550X (Quorum Technologies, United Kingdom) sputter coater.

2.4. Determination of drug release profiles *in vitro*

2.4.1. Drug content and drug release in physiological and tumour mimetic pH

To evaluate *in vitro* DOX release from the prepared DOX-OCP powders, 15 mg of three replicate samples from each DOX-OCP batch were immersed in 4 mL of PBS (pH 7.4 and pH 6.0) and incubated at 37 °C \pm 0.5 °C and 100 rpm (Environmental Shaker – incubator ES-20, Biosan, Riga, Latvia). The pH of PBS was adjusted with HCl. 2 mL aliquots of the solutions were taken directly from the vessels after 40 min, 2 h, 4 h, 6 h, 24 h, 48 h and 72 h and, finally, every seven days for a period of 42 days for pH 7.4 and for pH 6.0. The volume taken in both experiments was replaced with 2 mL of fresh corresponding solution, keeping the total dissolution medium volume constant. To determine the drug content in DOX-OCP, all samples were dissolved in the acidic water (pH 1.5 \pm 0.05, adjusted with HCl), at a solid to liquid ratio of 1 mg/1 mL and mixed with a vortex. DOX content in dissolution medium was determined using Ultra Violet-Visible spectrometry (UV–Vis, Evolution 300, Thermo Scientific, Waltham, MA, analysis software: VISION pro) at λ = 480 nm and expressed as the cumulative DOX release from the DOX-OCP powders.

2.4.2. Drug adsorption on octacalcium phosphate

DOX adsorption experiments on OCP were carried out using a single DOX to OCP ratio corresponding to the 9 wt% for 9DOX-OCP in the *in situ* methodology (100 mg of OCP, 9 mg of DOX). In order to compare 9DOX-OCP and 9DOX-OCP ads, total drug content was determined, and DOX release was tested for 48 h. The total amount of DOX (DOXads) was determined by dissolving it in the acidic water (pH 1.5 \pm 0.05, adjusted with HCl), at a solid to liquid ratio of 1 mg/1 mL and testing with UV–VIS at λ = 480 nm. The drug release of 9DOX-OCP ads was tested at pH 7.4, by following the same procedure described in the previous paragraph.

2.5. *In vitro* biological studies

2.5.1. Determination of IC50 and cytocompatibility

2.5.1.1. Cell culture. Cytotoxicity of 1DOX-OCP, 5DOX-OCP and 10DOX-OCP was tested on human-derived osteosarcoma cell line MG63 and mouse-derived preosteoblast cell line MC3T3-E1. Prior to the experiments, both cell lines were continuously cultured as described in ATCC product sheet. Briefly, MG63 cells were expanded in α -MEM medium supplemented with 10 % FBS and 1 % pen-strep. Similarly, MC3T3-E1 cells were cultivated in α -MEM medium supplemented with 10 % FBS and 1 % pen-strep. All cell lines were maintained at 37°C in a humidified atmosphere – 5 % CO₂.

2.5.1.2. Drug cytotoxicity. DOX stock solution was prepared by dissolving it in a dimethyl sulfoxide to achieve a high concentration (10 mM). Then, a series of DOX dilutions were prepared by diluting the stock solution with culture medium to obtain a range of concentration (0.1 nM to 1 μ M). The stock solution was sterilized through filtering by using 0.22 μ m syringe filter.

Each cell line was plated at a concentration of 1x10⁴ cells/well in 96-well plate, respectively. The plates were incubated in the incubator for 24 h to allow cell attachment and growth. After 24 h incubation period, the culture media was removed and the DOX dilutions were added by following the serial dilution protocol. The culture medium only (no DOX) was used as a control. Cells were treated with DOX dilutions for 24 h. After 24 h incubation, cell viability was assessed using cell-counting kit-8 (CCK-8). Absorbance was measured by using microplate reader (Infinite® 200 PRO, Tecan, USA) at 450 nm. The percentage of cell viability was calculated for each DOX concentration and for the control wells. A dose–response curve using the log-transformed DOX concentrations was plotted to calculate the IC50 level of DOX (DOX

concentration that causes 50 % inhibition of cell viability) on MG63 and MC3T3-E1 cell lines.

2.5.1.3. Cell viability assays. MG63 and MC3T3-E1 cells were cultured as described above. The cytotoxicity of DOX-loaded OCP powders (1DOX-OCP, 5DOX-OCP, and 10DOX-OCP) was assessed using indirect methods. Prior to cell seeding, DOX-loaded OCP powders were sterilized with 70 % ethanol for 40 min. 5×10^4 cells were seeded per well in a 24-well plate. Then, a cell strainer (VMR, USA) with a pore size of 0.4 μm , containing 3.75 mg DOX-loaded OCP powder, was placed in each well and incubated for 7 days. The powder/medium ratio (3.75 mg/mL) was maintained, as in the DOX release measurement experiment. Cell viability (%) was determined using the CellTiter-Blue™ assay, following the manufacturer's instructions. Briefly, CellTiter-Blue reagent was added to each well on day 1, 2, 3, 5, and 7, and incubated for two hours. After incubation, the CellTiter-Blue™ containing medium was transferred to a 96-well plate, and the absorbance was measured at 570 nm using a microplate reader (Infinite® 200 PRO, Tecan, USA), with 600 nm as the reference wavelength. Additionally, optical images of the cells were captured after 7 days of incubation to assess their morphology and overall growth.

2.5.2. Determination of cell death pathway

2.5.2.1. Cell culture and treatment. U2OS, MG63 and HOS osteosarcoma cell lines were maintained in DMEM supplemented with 10 % FBS, 2 mM L-glutamine and 1 % penicillin/streptomycin, and cultured at 37 °C in humidified incubator with 5 % CO₂. Cells were exposed to 3.75 mg/mL of 1DOX-OCP, 5.4 μM doxorubicin and 10 μM Ferrostatin-1.

2.5.2.2. Cell viability assays. Cell viability was measured using AlamarBlue™ reagent according to the manufacturer's instructions. Briefly, cells were plated in 24-well plates at a density of 15×10^3 cells/well. Cells were exposed for 48–72 h to 3.75 mg/mL of 1DOX-OCP or OCP alone in indirect contact, by using multiwell inserts. After treatments, the cell medium was discarded and an appropriate volume of AlamarBlue® reagent was added and incubated for up to 4 h. Fluorescence was monitored at 530–560 nm excitation wavelength and 590 nm emission wavelength, using a TECAN microplate reader (TECAN, Switzerland).

2.5.2.3. qRT-PCR. TripleXtractor reagent was used to isolate total RNA, as indicated by the supplier. The ExcelRT™ Reverse Transcription Kit was used to synthesize cDNA, following the manufacturer's instructions, by using 2 mg of total RNA. Quantitative PCR reactions were performed by using a CFX96 thermocycler. Primer sequences are reported in Table 2 and were designed by using the online IDT PrimerQuest Tool software (IDT; <https://eu.idtdna.com/Primerquest/Home/Index>). The L34 mRNA level was used as an internal control, and the comparative Ct method (DDCt) was used for the relative quantification of gene expression (Gagliardi et al., 2023).

2.5.2.4. Western Blotting analysis. Proteins were isolated by using a RIPA Buffer supplemented with a protease inhibitor cocktail. An equal amount of proteins (20 μg) were subjected to an SDS-PAGE and electroblotted onto nitrocellulose membranes (Bio-Rad). Membranes were blocked for 1 h by using 5 % non-fat dry milk in PBS plus 0.1 % Tween20 and incubated with indicated primary antibodies in a blocking solution,

Table 2
Primer sequences.

Target	Sequence: Forward/Reverse
CHAC1	CTCAAGCGCTGTGGATTT/TGCTCCCTGCCAGAAA
ACSL4	CCTGCAGCCATAGGTTAAAG/CAGGCCAGTGTGAAAGAATA
PTGS2	GCCTGGTCTGATGATGTATG/GTATTAGCCTGCTTGTCTGG
L34	GTCCCGAACCCCTGGTAATAGA/GGCCCTGCTGACATGTTTCTT

overnight at 4 °C. Primary antibodies were: anti-cleaved PARP (1:1000); anti-Tubulin (1:1000). Detection was achieved using HRP-conjugated secondary antibodies (1:5000) and visualized by SuperSignal West Pico Plus (ThermoFisher). Images were acquired by using a ChemiDoc Touch Imaging System (Bio-Rad) and analyzed by Image Lab software (Bio-Rad).

2.6. Statistical analysis

Each group of samples was represented by three or six replicates. All the synthesis have been done more than five times to show the repetitive formation pathway. Where applicable, results were presented as mean value \pm standard deviation.

When comparing groups of samples, analysis was performed in Prism (v8, GraphPad Software, USA), using the one-way ANOVA, Tukey's post hoc analysis and normal distribution Shapiro-Wilk's test. The difference was considered significant for $p < 0.05$. All the experiments were performed in triplicate, and data values were presented as means \pm standard deviations. Viability data were analysed using the two-way ANOVA and then Tukey's multiple comparison test. P-values of < 0.05 were considered to indicate statistical significance.

3. Results and discussion

With their exceptional bioactivity and tailorable biodegradability, calcium phosphates have been standing out from other biomaterials, which made them an excellent choice for drug delivery in biomedical applications, orthopaedics and dentistry. OCP is reckoned to possess a higher affinity towards organic molecules than other CaPs (Yang et al., 2010). This is owing to the particular arrangement of the structure, crystallographic planes and a relatively empty water layer, where the incorporation of distinct ions and molecules is much more achievable. The interchangeably arranged structure made of an apatite layer of 1.1 nm–resembling the main attributes of HAp, and a water layer, comprised of ten water molecules (H₂O) in the unit cell of 0.8 nm, mimic a channel going lengthways with the c-axis (Kovrljija et al., 2021). Furthermore, it has been hypothesized that, if the drug loading is implemented *in situ* in the first steps of the OCP synthesis, it can lead to ultrahigh drug loading capacity, ensuring a prolonged drug release (Tang et al., 2011). This is mainly because of the numerous binding sites that are resulting from CaP clusters, which have an ultrahigh specific surface area, giving the possibility for the drug molecules to be adsorbed on the surface. In our previous work (Kovrljija et al., 2023) we have shown that during the hydrolysis process, α -TCP transforms to OCP through several steps: dissolution, precipitation and the growth step of OCP phase. As these steps in the mechanism imply a release of hydroxyl ions (OH⁻) and orthophosphate anions (HPO₄²⁻), their subsequent role in the formation of the hydrated layer in the OCP led us to assume that incorporating the DOX during the *in situ* OCP synthesis process, could potentially lead to the drug loading in the hydrated layer itself.

3.1. Synthesis and characterization of doxorubicin loaded octacalcium phosphate

Being a metastable phase, OCP formation depends on multiple factors and it is not easy to obtain a final pure product without impurities (e.g., brushite) that are present in its transformation process (Kovrljija et al., 2023). Due to this, the first step was to establish the thermal transformation of ACP to α -TCP to be certain that the sintering has yielded pure α -TCP (Fig. 1A in supplementary file (Fig. 1A S)). Subsequently, pure OCP has been synthesized from the low temperature α -TCP and used as a reference material for the final step of creating the DDS with OCP and varying contents of doxorubicin.

3.1.1. Formation of α -TCP and pure OCP

Thermal transformation of ACP to α -TCP was confirmed using XRD

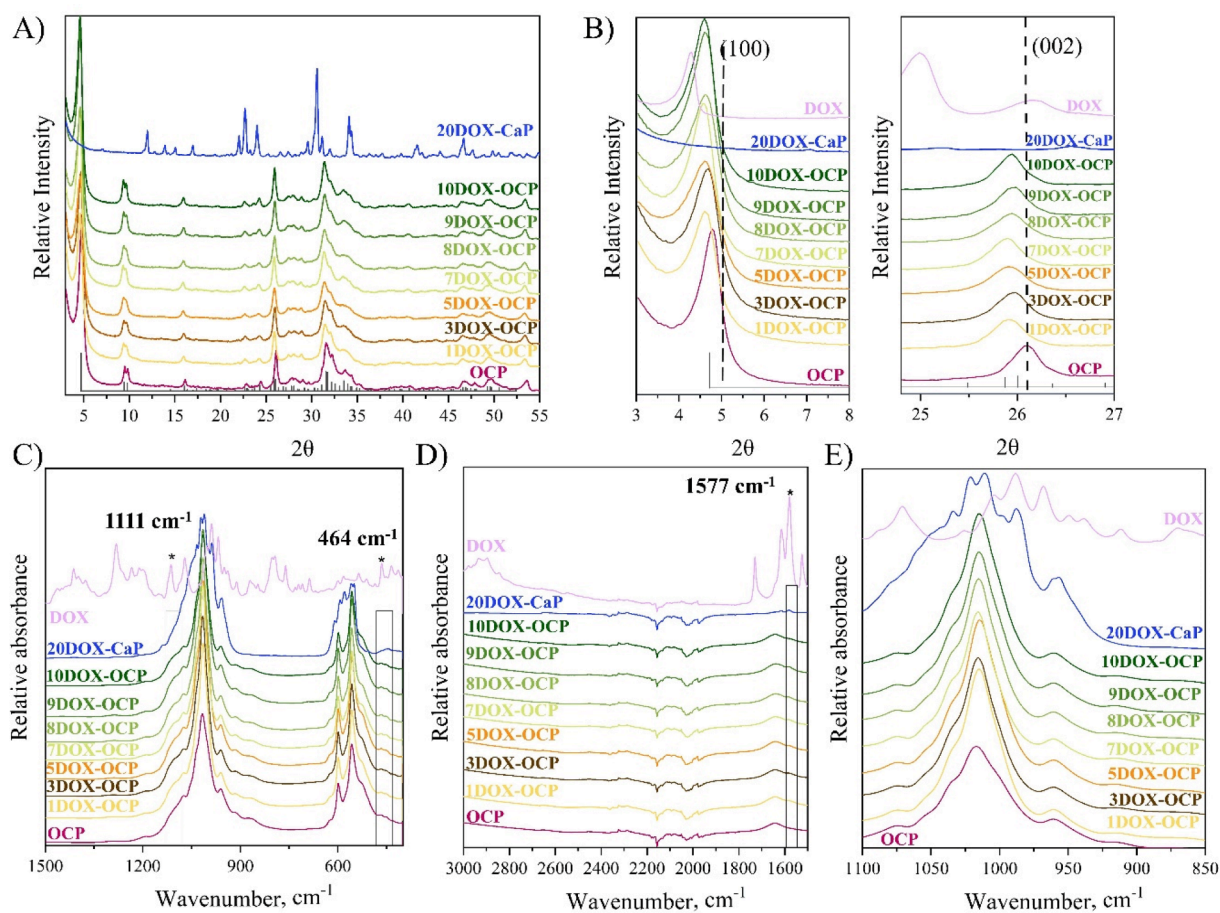


Fig. 1. Characterization of OCP and DOX-OCP (1 – 20 wt%): A) XRD patterns; the reference simulated pattern (ICDD entry #026–1056) corresponds to OCP triclinic phase. B) XRD patterns of OCP and DOX-OCPs. Maxima at 4.7 and 26.1 2θ degrees are respectively attributed to the planes (100) and (002) of OCP crystal. C, D, E) FTIR spectra of DOX-OCP. Star and the combining brackets mark the bands that have changes due to DOX incorporation.

analysis (Fig. 1A in supplementary file (Fig. 1A S)). Representative maxima of α -TCP were in agreement with the reference XRD pattern provided by the ICDD, while FTIR spectroscopy analyses clearly showed the specific α -TCP bands ($1300\text{--}900\text{ cm}^{-1}$ domain and $700\text{--}500\text{ cm}^{-1}$ domain, attributed to the vibrations of PO_4^{3-}) found in the spectra (Fig. 1B S). SEM micrographs (Fig. 1C S) displayed the morphology of α -TCP agglomerates with elongated grain like particles (sizes below 500 nm).

Using α -TCP as the only precursor, OCP was synthesized via hydrolysis process, within 24 h. The XRD pattern, FTIR spectra and SEM corroborated the formation of pure OCP from α -TCP (Fig. 1D S, 1E S, 1F S, respectively).

3.1.2. Doxorubicin loaded OCP

In order to attain the highest possible drug loading, doxorubicin was added *in situ*, at the beginning of the α -TCP hydrolysis. However, as it was shown before with other ions/drugs added to OCP (Kovrlija et al., 2021), loading can be done up to a certain extent, after which the formation of OCP can be inhibited. With this limitation, two questions have been acknowledged: can DOX be loaded into OCP and how much of it can be added to have the OCP phase?

3.1.3. X-Ray Diffraction

DOX was added in the range from 1 wt% to 20 wt% of the total starting amount (Table 1). DOX-OCP phases were attained after 24 h (Fig. 1 A)). Once the syntheses have been performed successfully and OCP particles with 1, 3, 5, 7, 8, 9 and 10 wt% (theoretical loading) of doxorubicin were obtained, XRD analysis have confirmed the

characteristic OCP fingerprints, proving that the mechanism of α -TCP conversion was still possible (Fig. 1 A). All X-ray diffraction peaks observed at low angles are characteristic to the OCP triclinic structure. Low angle (100) maximum, at $2\theta = 4.7$ degrees and a doublet (200) and (010) at 9.4 and 9.7 degrees, respectively, were clearly seen (Fig. 1 A)(Kovrlija et al., 2023). If compared with pure OCP, DOX-OCP diffractograms exhibited a slight shift towards the lower 2θ degrees (Fig. 1B). Slight shift of the 4.7 and 26.1 2θ degrees maxima, respectively, attributed to the planes (100) and (002) of OCP crystal, indicated the lattice expansion in the DOX-OCP system (Fig. 1 B). Moreover, obtained results revealed, that the crystal structure of OCPs was slightly altered with the increasing DOX content, according to the changes of diffraction angle and peak intensity (Fig. 1B). While not a definitive confirmation of DOX integration into the OCP structure, the shifted main maxima observed at 4.3, peaks at 10.1, 16.5, 26.20, and a pattern spanning from 30.1 to 36.5 2θ degrees, suggest a potential for significant influence. It was also shown that the stabilization of the OCP structure was dependent on the amount of DOX used for the OCP-DOX synthesis. If the amount was above 10 wt% (theoretical loading), it led to the inhibition of the c-axis growth and the destabilization of the overall transformation mechanism, leaving the drug adsorbed on the α -TCP phase (Fig. 2 S and Fig. 1 A and B). The concentrations of DOX between 10 and 20 wt% (12, 15 and 18 wt%) have all inhibited the OCP formation (Fig. 2 S), and for further *in vitro* analysis 20DOX-OCP has been chosen as a representative of them. The most significant maxima for α -TCP remained in 20DOX-OCP (12.1, 30.7 2θ degrees, with double maxima ~ 22.8 and ~ 34 2θ degrees) (Fig. 1 A and B).

To test the difference between the synthesis methodologies and to

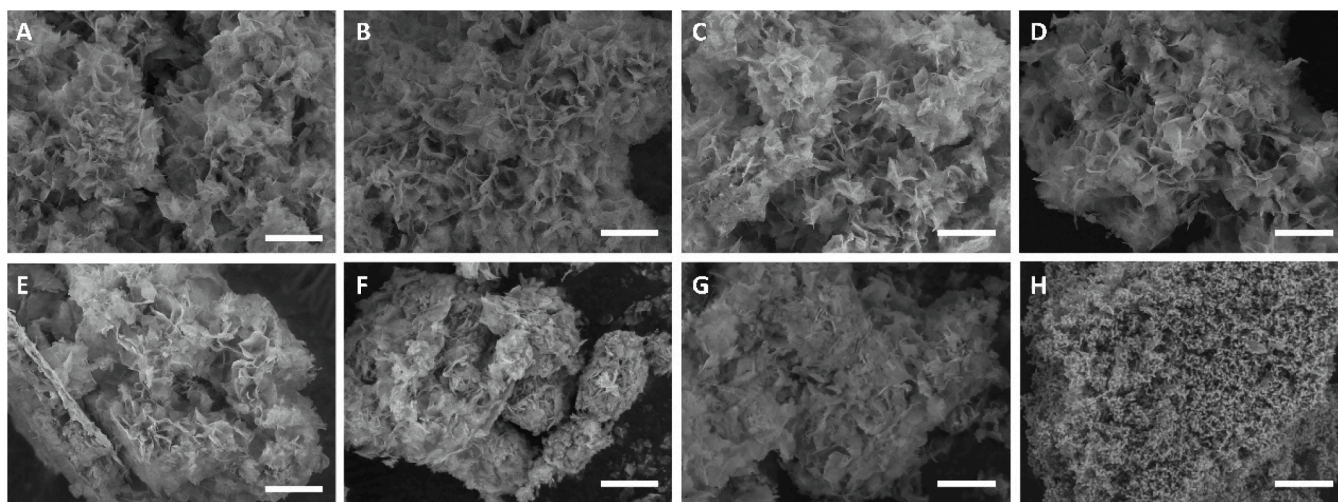


Fig. 2. Characterization of OCP and DOX-OCP (1–10 wt%) and DOX-TCP (20 wt%): SEM micrographs (a–1 wt%, b–3 wt%, c–5 wt%, d–7 wt%, e–8 wt%, f–9 wt%, g–10 wt% and h–20 wt%); scale bar 5 μm bottom right.

confirm whether the *in situ* strategy resulted in DOX being incorporated in OCP, adsorption experiment has been done. By mixing OCP with the DOX solution, no significant changes have been noticed in the crystallographic pattern of OCP (Fig. 3 S). Previously observed peak shift of the characteristic maxima in 9DOX-OCP synthesized *in situ* (4.7 and 9.4 and 9.7 2θ degrees), which was an indication of DOX incorporation within the water layer, has not been seen in 9DOX-OCP ads. That suggested that DOX was solely adsorbed on the material's surface. The most noticeable change within 9DOX-OCP ads was pronounced maxima at ~ 31 and 45 2θ degrees, which have been assigned to the sodium chloride (NaCl) that was present in the PBS (Fig. 3 S).

3.1.4. Fourier Transform Infrared Spectroscopy

To corroborate the structural identification, FT-IR spectroscopy has been completed on all of the samples. Assignment of the presence of the hydrogen phosphate (HPO_4^{2-}) and phosphate (PO_4^{3-}) groups is of crucial value when establishing the OCP phase. All of the samples, except 20DOX-CaP, have representative markings of the OCP phase (Fig. 1C). The $\text{PO}_4^{3-} \nu_3$ stretching mode encompassing the bands at 1077 cm^{-1} , 1296 cm^{-1} and 1120 cm^{-1} has been accentuated. Additionally, $\text{PO}_4^{3-} \nu_4$ domain of the OCP spectrum showed the characteristic absorbance bands at 524 , 560 , 601 and 627 cm^{-1} . More importantly, P-OH

stretching at 917 cm^{-1} and 861 cm^{-1} , connected with the HPO_4^{2-} ion has been prominently distinguished. Same as in XRD data, 20DOX-CaP exhibited clearly the markings of α -TCP with strongest bands found in 1300 – 900 cm^{-1} and 700 – 500 cm^{-1} domain, attributed to the vibrations of PO_4^{3-} . To some extent, the influence of strong DOX absorbance bands can be seen in DOX-OCP systems. Increasing intensity of the band in the region 1570 cm^{-1} indicates an antisymmetric COO stretch. DOX prominent peak at $\sim 1111 \text{ cm}^{-1}$ led to the broadening of the $\text{PO}_4^{3-} \nu_3$ stretching domain when compared to OCP and as a result, slight shoulder band can be distinguished in DOX-OCP systems (Fig. 1C). The band at 464 cm^{-1} (Fig. 1C) from DOX could indicate the traces in the composition of all the DOX-OCP samples, as the increase in the intensity of the band is gradually higher with the increase of the drug load. The bands assigned to $\text{HPO}_4(5)$ at 1193 cm^{-1} in OCP were reduced to a weak band at DOX-OCPs, indicating that the $\text{HPO}_4(5)$ group is substantially reduced. However, most of the bands only had a slight broadening, with a high possibility of auxiliary convoluted bands underneath the main ones, hindering the possibility of clearly marking the peaks of DOX (Fig. 1C). Another possible explanation to the changes in the chemical structure could be the formation of DOX/ Ca^{2+} complexes. The oscillation of the aromatic ring (C–H oscillations derived from aliphatic groups (e.g., methoxy groups)) occurs throughout the spectral range and also in the areas where slight changes have been noticed in DOX-OCPs (~ 1580 – 1600 cm^{-1}). Moreover, the divalent metal-DOX complexes showed the ring breathing and bending vibrations of C(16)–C(18) = O, C(30)–H3 at $\sim 1000 \text{ cm}^{-1}$ (Jablonska-Trypuc et al., 2017).

3.1.5. Surface morphology

Particular OCP plate-like morphology makes it easy to distinguish between HAp and α -TCP. Plate crystals usually have a strong tendency to assemble into a rose-like form; however, the size of such an agglomerate varies among different samples, where OCP thin plates did not exceed $2 \mu\text{m}$ (Fig. 2). During the *in situ* incorporation of DOX, plate-like particles seemed to be more overlapping and entwining with the increase of DOX amount in samples, subsequently leading them to form agglomerates from 1 to $20 \mu\text{m}$ (Fig. 2 A–G). However, there is no definite indication that this is due to the DOX presence within the system. The highest wt% of incorporated DOX (20 wt%) led to the inhibition of OCP plate like structure and preservation of elongated grain-like particles typical for α -TCP (Fig. 2 H).

3.2. Evaluation of DOX release kinetics from DOX loaded OCP particles

Ever since it was approved by the Food and Drug Administration

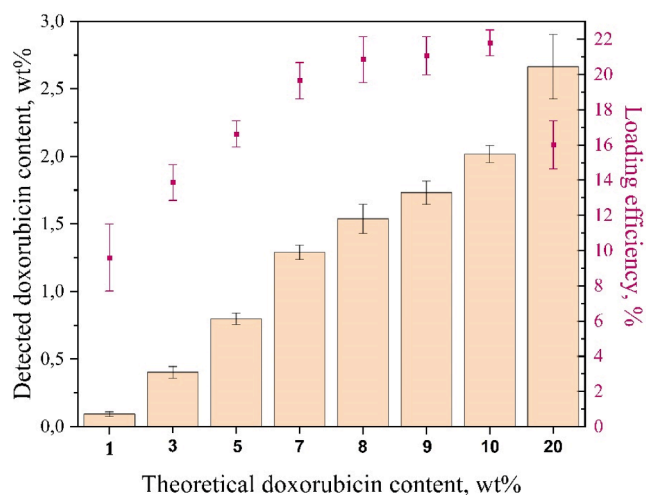


Fig. 3. Total DOX content and DOX loading efficiency in OCP-DOX samples (1–10 wt%), and in DOX-TCP sample (20 wt%).

(FDA) in 1974 (Sriharan & Sivalingam, 2021), DOX was used in many combinations with multiple intracellular targets. When intravenously administered DOX had an initial half-life of 8 min and a terminal half-life of 30 h, while plasma clearance of doxorubicin was 324–809 mL/min/m², and the effect on DNA has been seen in concentrations as low as 10 nM. Nevertheless, the dosage amounts vary depending on the site of usage and overall conditions (e.g., *in vitro*: 2 μM/5 μM for 24 h, *in vivo*: 5 mg/kg/dose, every 15 days (Sriharan & Sivalingam, 2021)). Due to these limitations of short half-life and systemic poisoning, local drug delivery vehicles are highly sought after. CaP therapeutic functionalisation to treat bone diseases became very attractive because of its ability to incorporate and retain the active substance while providing a way to deliver it locally in a controlled manner. DOX adsorption experiments on apatite substrates showed that DOX molecules did not have a high affinity for the surface of apatite and the amount of DOX adsorbed was 8 μmol DOX m⁻² apatite (Iafisco et al., 2016). When DOX was incorporated into bone cements, contradictory data was seen. One group observed a sustained and controlled release (Tani et al., 2006), while Genin et al. recorded a burst release for the first 40 h that continued to a prolonged release up to 240 h (25 % DOX after 40 h and 35 % after 240 h) (Génin et al., 2004; Pylostomou et al., 2023).

The effect of the *in situ* incorporation of doxorubicin into OCP had a detrimental impact on the amount of the incorporated DOX, as well as on the cumulative drug release. As expected, the obtained results showed that with an increase of theoretical DOX content in the OCP, the detected incorporated drug content and the loading efficiency increased gradually (Fig. 3). In the case of DOX content of 1, 5 and 10 wt% (theoretical loading), the amount of detected incorporated DOX was

0.093 ± 0.01 wt% with the loading efficiency 9.6 ± 1.9 %, 1.54 ± 0.1 wt% with the loading efficiency 20.85 ± 1.29 % and 2.02 ± 0.06 wt% with the loading efficiency 21.8 ± 0.73 %, respectively.

However, with DOX loading of 20 wt%, which did not yield the OCP phase, the highest incorporated DOX amount was observed (2.66 ± 0.24 wt%), but the loading efficiency was quite low (15.99 ± 1.36 %). A possible reason could be that DOX was adsorbed on the surface of α-TCP, thus at the same time inhibited the OCP formation and showed a higher detected drug content.

The *in vitro* release of doxorubicin from the DOX-OCP system in pH 7.4 and pH 6.0 is shown in the Fig. 4. Early DOX burst release, observed initially in the first 24 h up to three days for pH 7.4, ranged from approximately 17 % to 75 % (Fig. 4A), while the continued and uniform release was monitored up to six weeks (Fig. 4B). The plateau of the cumulative release percentage was inversely proportional to the theoretical content of doxorubicin. For example, for 5DOX-OCP, 23.6 ± 1.6 % (28.0 ± 3.7 μg) was released after two hours, 38.9 ± 1.3 % (46.3 ± 4.2 μg) after 72 h and 52.5 ± 2.3 % (62.3 ± 5.8 μg) after 42 days. While, the 10DOX-OCP reached 15.9 ± 1.3 % after two hours, 27.7 ± 1.7 % after 72 h and 38.3 ± 2.0 % after 42 days. It was noticed that the lower the amount of the incorporated doxorubicin, the higher the release rate. This observation could be caused by the phase transformation of OCP to calcium deficient hydroxyapatite. Lower amounts of drug may result in faster transformation, which could consequently lead to a faster release (Ito et al., 2014). Except for 1DOX-OCP, all other tested samples have not completely released the active substance, indicating that the drug release period can be substantially longer. In general, increasing the concentration of the drug loading increased the adsorbed amount of

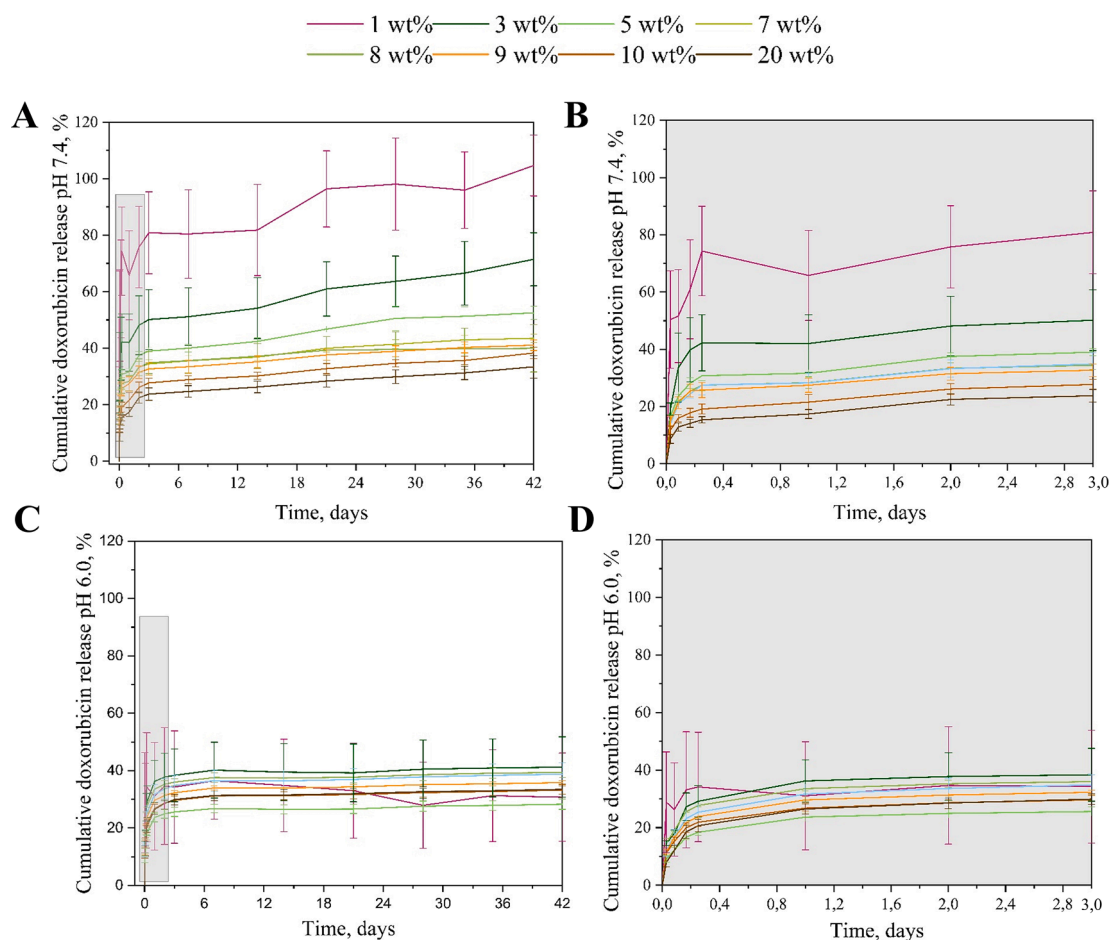


Fig. 4. Doxorubicin doped OCP: A) total doxorubicin release during six weeks (%) pH 7.4 and B) doxorubicin initial burst release in the first 72 h (%) pH 7.4C) total doxorubicin release during six weeks (%) pH 6.0 and D) doxorubicin initial burst release in the first 72 h (%) pH 6.0.

drug until a certain threshold. In our case, even though the amount of the detected incorporated DOX content increased with the addition of 20 wt% of the drug (Fig. 3), the obtained DDS was not considered successful as it prevented the formation of OCP.

The *in vitro* release of doxorubicin from the DOX-OCP system in the tumour mimetic environment (PBS pH 6.0) showed a similar trend for the higher amounts of loaded doxorubicin (7, 8, 9, 10 and 20 wt%), whereas for the lower amounts the release was slower (1, 3 and 5 wt%). Early DOX burst release, observed initially in the first 24 h up to three days, ranged from approximately 23 % to 39 % (Fig. 4D), while the continued and uniform release was monitored up to six weeks (Fig. 4C). For example, 5DOX-OCP released 12.1 ± 0.9 % (20.4 ± 1.6 μ g) of DOX after two hours, 25.6 ± 1.6 % (42.9 ± 3.2 μ g) after 72 h and 52.5 ± 2.3 % (47.4 ± 4.0 μ g) after 42 days. While, the 10DOX-OCP had almost the same release, reaching 15.3 ± 1.3 % after two hours, 29.6 ± 1.5 % after 72 h and 33.1 ± 1.4 % after 42 days. The slower release (and similar release) trend of DOX-OCPs in pH 6.0, could be connected with the stability of OCP in the acidic solutions. OCP's transformation to apatite is solution mediated and guided by factors such as pH, temperature, ionic concentration, time etc. In acidic pH, OCP is stable, except when the solution contains fluoride ions (LeGeros et al., 1989). As we assume the partial release of the drug from DOX-OCP DDS is due to the gradual transition of OCP to apatite, if that transition is hindered the release would be either similar or slower (in case of the small amounts of the drug being incorporated).

In the literature, the mechanism of adsorption and parameters of several models are being attuned to fit the experimental curves, i.e. isotherms of drug adsorption, out of which the most common ones are Langmuir's and Freundlich's (Parent et al., 2017). If the detected quantity of the drug increases gradually with the drug concentration, which was the case in our DDS, it follows Freundlich's isotherm. This potentially indicates that the prospective carrier sites of adsorption stay unsaturated. The initial burst release of DOX within the first six hours continued until day three in a decreased trend, and then it stabilized and continued for the following 39 days. One way to control the initial drug release would be to incorporate the DOX carrier into a polymer, thus creating a more complex DDS (Pelss et al., 2011). Physical adsorption of the doxorubicin molecules to the surface of OCP, through electrostatic forces or hydrogen bonding, between the positively charged DOX molecules and negatively charged OCP could explain the initial burst release. Whereas, the sustained DOX release afterwards could be clarified through strong chemical interaction (Ca–O) that can hamper the escape of the drug from the DOX-OCP drug delivery system. Similar behaviour was noticed by Zhu et al (Qi et al., 2015) when they loaded amorphous calcium phosphate (ACP) with doxorubicin and tested the ACP/DOX DDS in PBS solution, at different pH values. Doxorubicin release was found to be low and they reached a plateau (1.7 %) over a period of 13 h. Jiang et al. (Xiaodan Jiang et al., 2022) tested the release of DOX from hydroxyapatite and also confirmed a quick release during the initial immersion period, followed by the slowly sustained release during the later immersion period (36.5 % at pH 7.4 after 100 h). To test the difference in release between the incorporated doxorubicin via the *in situ* method and doxorubicin adsorbed onto the OCP, 9DOX-OCP ads was immersed in PBS pH 7.4 and observed for 48 h. The initial detected amount of DOX was higher in 9DOX-OCP ads (3.07 ± 0.4 %) than in 9DOX-OCP (1.7 ± 0.1 %). In the first 6 h, 48.3 ± 2.2 % of DOX was released, while at 48 h the detected amount was 51.1 ± 2.8 % (Fig. 4 S). In comparison to the 9DOX-OCP, where DOX was integrated through *in situ* synthesis, only 25.7 ± 2.6 % of DOX was released at the 6th hour, with the total release reaching only 31.5 ± 2.2 % on the second day. This clearly confirmed the effectiveness of the *in situ* method. *In vitro* release evaluations are not envisioned to predict the *in vivo* release, but they rather aim to advance the overall knowledge regarding the parameters inducing the DDS compartment and to give an indication of the set-up of the initial *in vitro* biological screenings.

3.3. *In vitro* cell studies

3.3.0.1. IC₅₀ and Cellular Response

The IC₅₀ values were drawn from the DOX dose–response curve of each cell line (Fig. 5). Accordingly, more than 0.85 ng (0.016 μ M) and 3.397 ng (0.062 μ M) of DOX is having an inhibitory effect for MG63 and MC3T3-E1 cells, respectively.

The influence of DOX release on the viability of MG63 and MC3T3-E1 cells was tested by placing OCP and DOX-loaded OCP powders in contact with cells by using inserts (Fig. 6). The culture medium incubated with DOX loaded OCPs (5DOX-OCP and 10DOX-OCP) suppressed MG63 and MC3T3-E1 cells in the period of 7 days. However, from day 3 to day 7 of culturing, the pure OCP showed a proliferative effect on both cell lines, resulting in increased cell viability (from 72.70 % to 84.89 % for MG63 cells and from 62.34 % to 96.84 % for MC3T3-E1 cells). The inhibition rate of 10DOX-OCP on the cell viability was significantly higher than that of the 5DOX-OCP and 1DOX-OCP, providing the additional evidence of their pronounced inhibitory effect on MG63 cells (Fig. 6 (a)). These *in vitro* cell studies also demonstrated that a time and concentration-dependent decreasing proliferation rate of MG63 and MC3T3-E1 cells was more evident with 5DOX-OCP and 10DOX-OCP (Fig. 6). With both formulations, the rate of viable cells after 72 h was dramatically low (30.81 ± 0.34 and 17.84 ± 0.09 for MG63 cells and 36.93 ± 1.27 and 24.19 ± 3.22 for MC3T3-E1 cells, respectively). MG63 viability decrease, when exposed to DOX-OCPs, could be solely attributed to the cytotoxic effects of DOX. DOX is known to interfere with DNA replication and induce cell death in various cancer cell lines (Akutsu et al., 1995; Roncuzzi et al., 2014; Wen et al., 2018). In this case, the DOX-loaded OCP powders likely released DOX molecules into the surrounding culture medium, which then interacted with the MG63 cells and caused a decrease in their viability. On the other hand, the increase in viability of MC3T3-E1 cells after 72 h could be due to several factors. MC3T3-E1 cells may have different characteristics or mechanisms that make them more resistant to the cytotoxic effects of DOX compared to the MG63 cells (Fig. 5). It is known that different cell lines can vary in their sensitivity or resistance to chemotherapy drugs, including DOX. Factors such as variations in drug uptake, efflux pumps, DNA repair mechanisms, cell cycle regulation, and apoptotic pathways can influence a cell line's response to cytotoxic agents (J. Wang et al., 2009). Furthermore, the presence of elevated Ca²⁺ ions in the medium could potentially activate the extracellular calcium-sensing receptor (Thorn et al., 2011). This activation, in turn, may enhance the proliferation of the cells. If the DOX created a Ca-complex with the CaP in the proposed DDS, the literature data have shown that the complexation of doxorubicin with metal ions has the ability to increase the cytotoxic properties of the drug (Jablonska-Trypuc et al., 2017). It has been shown that complexes with Fe³⁺ and Cu²⁺ ions facilitate the binding of doxorubicin to DNA and increase the production of reactive oxygen species, which aids in the cytotoxic effect. However studies also have shown that doxorubicin can form DNA double-stranded breaks in human cells enabling the calcium channel blocker to sensitize cells to doxorubicin and dampen the doxorubicin efficacy (Thuy et al., 2016). Moreover, the observation of comparable or increased viability levels of the OCP powder in comparison to the control group indicated that the uptake of Ca²⁺ ions, which play a crucial role in osteointegration, positively influenced cell proliferation.

Phase-contrast micrographs showed that after 7 days of incubation, the majority of MG-63 cells on the plate incubated with DOX-OCPs were dead, remaining rounded and small in size, indicating an inhibitory effect of DOX (Fig. 6 (c)). In comparison, the control group and OCP powders appeared to result in more spread-out cell lines. The introduction of OCP powders into the cell medium significantly improved cell adhesion, as seen from the polygonal morphology of the cells. The largest cells were observed in the control group.

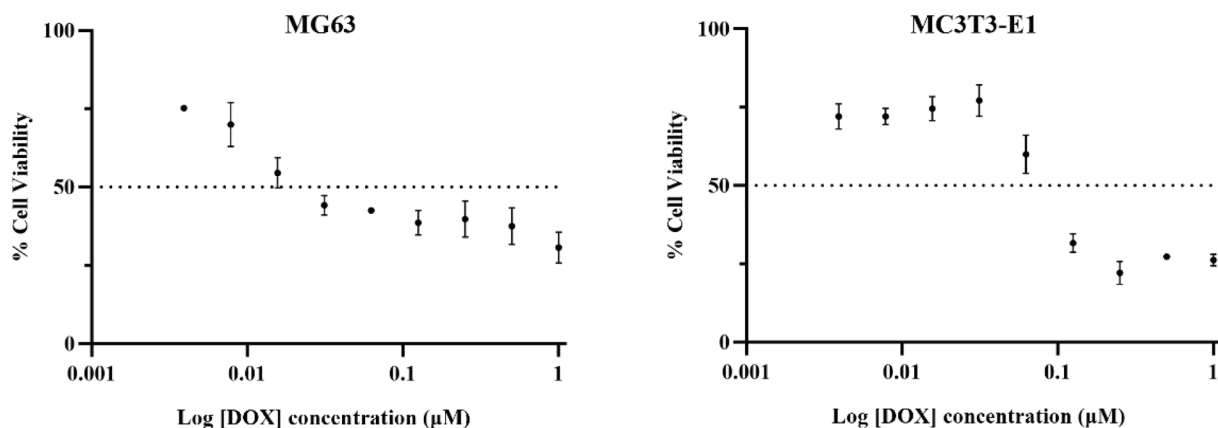


Fig. 5. Comparison of the sensitivity to doxorubicin of the MG63 and MC3T3-E1 cell lines. Cell viability was measured using CCK-8 assay to determine the IC_{50} (μM) of doxorubicin in MG63 (a) and MC3T3-E1 (b) cells after treatment with different concentrations of doxorubicin for 24 h. Error bars indicate the standard deviations ($n = 3$).

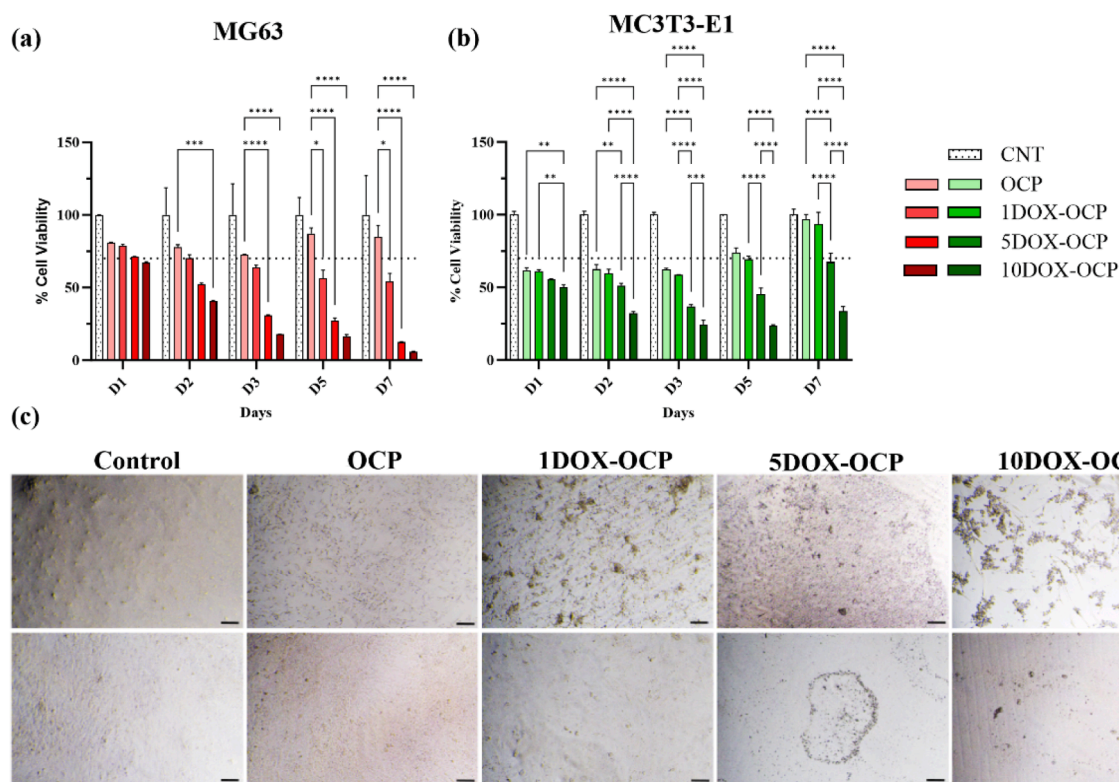


Fig. 6. Cell viability studies of DOX-loaded OCP powders. (a) Cell viability assay of MG63 cells and (b) MC3T3-E1 cells with OCP, 1DOX-OCP, 5DOX-OCP and 10DOX-OCP powders. The dotted line in (a) and (b) represents the viability limit at 70 %. This means that if the viability of cells falls below 70 %, the released drugs or ions are considered toxic. Error bars indicate the standard deviations ($n = 3$). Statistically significant differences: * for $p < 0.05$ ** for $p < 0.005$, *** for $p < 0.001$, **** for $p < 0.0001$. (c) Phase-contrast images of cell morphology after 7 days of cultivation in different powders. Scale bar indicates 10 μm .

3.3.0.2. Pathway of cell death

To evaluate the anticancer properties and the pathway of cell death induced by 1DOX-OCP, a panel of three human osteosarcoma (OS) cell lines was used. U2OS, HOS, and MG-63 cells were exposed to 3.75 mg/mL 1DOX-OCP or 3.75 mg/mL OCP. 5.4 μM of doxorubicin (DOX), corresponding to the estimated drug released by 1DOX-OCP within 72 h, were used as a positive control. Firstly, cell viability was evaluated after 72 h, in cells stained with AlamarBlue. As in the previous cytocompatibility tests, results indicated a significant decrease in the viability of all tested osteosarcoma cells upon exposure to 1DOX-OCP (Fig. 7). The observed differences in cell viability between 1DOX-OCP and DOX could result from the immediate availability of the drug at the final

concentration in the positive control group (DOX), whereas doxorubicin from 1 wt% of OCP-DOX was released gradually in a time-dependent manner, which corresponded to the *in vitro* drug release study (Fig. 4).

In the second stage, the three cell lines were exposed to 3.75 mg/mL of 1OCP-DOX, 3.75 mg/mL of pure OCP, or 5.4 μM doxorubicin (DOX), and the expression of the three well-known ferroptotic markers, such as CHAC1, ACSL4 and PTGS2 (Chen et al., 2021) was evaluated after 48 h by qPCR. Results indicated significant upregulation of all three genes only in HOS cells exposed to 1DOX-OCP (Fig. 5 S). Then, in order to verify if OCP-DOX induces ferroptotic cell death, OS cells were exposed for 72 h to 3.75 mg/mL of 1DOX-OCP and 5.4 μM DOX alone or in combination with the ferroptosis inhibitor Ferrostatin-1 (Fer-1) (Miotto

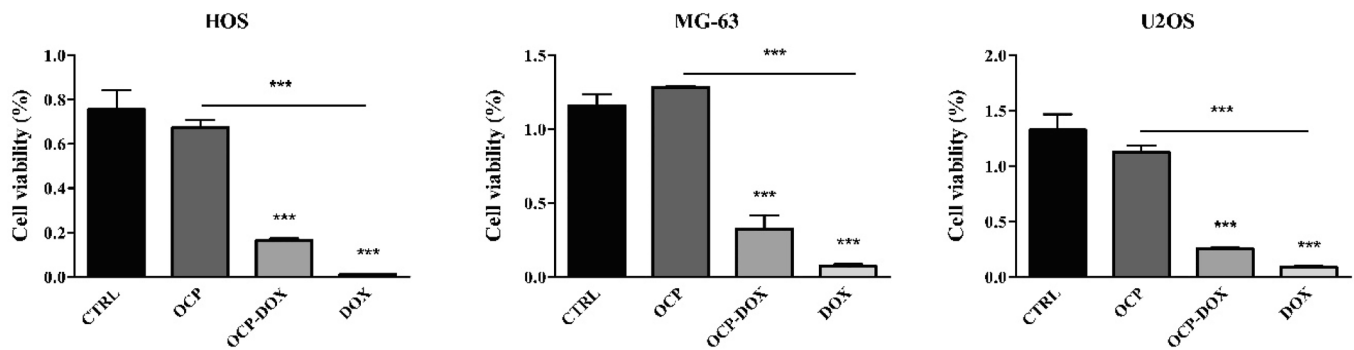


Fig. 7. Sensitivity of OS cells to DOX-loaded OCP powder. The indicated OS cell lines were exposed 72 h to 1DOX-OCP, pure OCP and doxorubicin (positive control). Cell viability was evaluated in AlamarBlue-stained cells. Histograms represent mean \pm s.d.; n = 3; ***p < 0.001.

et al., 2020). Cell viability evaluated in AlamarBlue-stained cells revealed no significant changes in OS cell survival in the presence of 1OCP-DOX + Fer1 compared to 1OCP-DOX alone (Fig. 8 A). These results indicated that ferroptosis is not involved in OCP-DOX-induced cell death in OS cells.

Next, we investigated the involvement of the conventional pathway of doxorubicin-induced PCD, apoptosis (S. Wang et al., 2004). To this aim, U2OS, HOS, and MG-63 cells were exposed to 1DOX-OCP, and levels of cleaved PARP, considered as a hallmark of apoptosis (Chaitanya et al., 2010), were evaluated after 48 h of treatment, by western blotting analysis. Results shown in Fig. 8 B indicate increased expression of cleaved PARP in HOS and MG-63 cells exposed to 1OCP-DOX, confirming the induction of apoptotic cell death.

Collectively, our results confirmed the anticancer effects of OCP-DOX, indicating that apoptosis is the main pathway of programmed cell death responsible for its cytotoxic effect on osteosarcoma cells.

4. Conclusions

Even though functionalized OCP crystals revealed a high potential and are assumed to be the future of tailored DDSs, the paucity of evidence on the comprehensive release profile *in vitro*, the aftermath of the *in vivo* settings and their relationship and implications is evident. The presented findings offer new insights into the design of DOX-loaded OCP, and their usage as potential drug vehicles, with satisfying drug loading capacity and sustained release behavior.

In situ loading of DOX-OCP has shown that for the first time it was possible to incorporate the doxorubicin into octacalcium phosphate, while maintaining its characteristic crystal structure. The maximum possible loading that was achieved was 10 wt%, theoretical drug load and the detected DOX content was 2.02 ± 0.06 wt% with the loading efficiency 21.8 ± 0.73 %. Furthermore, it was proven that everything above 10 wt% inhibited the OCP formation. With the developed DOX-OCP systems, the two out of three benefits of OCP's triple effect (discussed in the Introduction section) have been seen: 1) the initial drug that was adsorbed on the surface of OCP was released at first and is

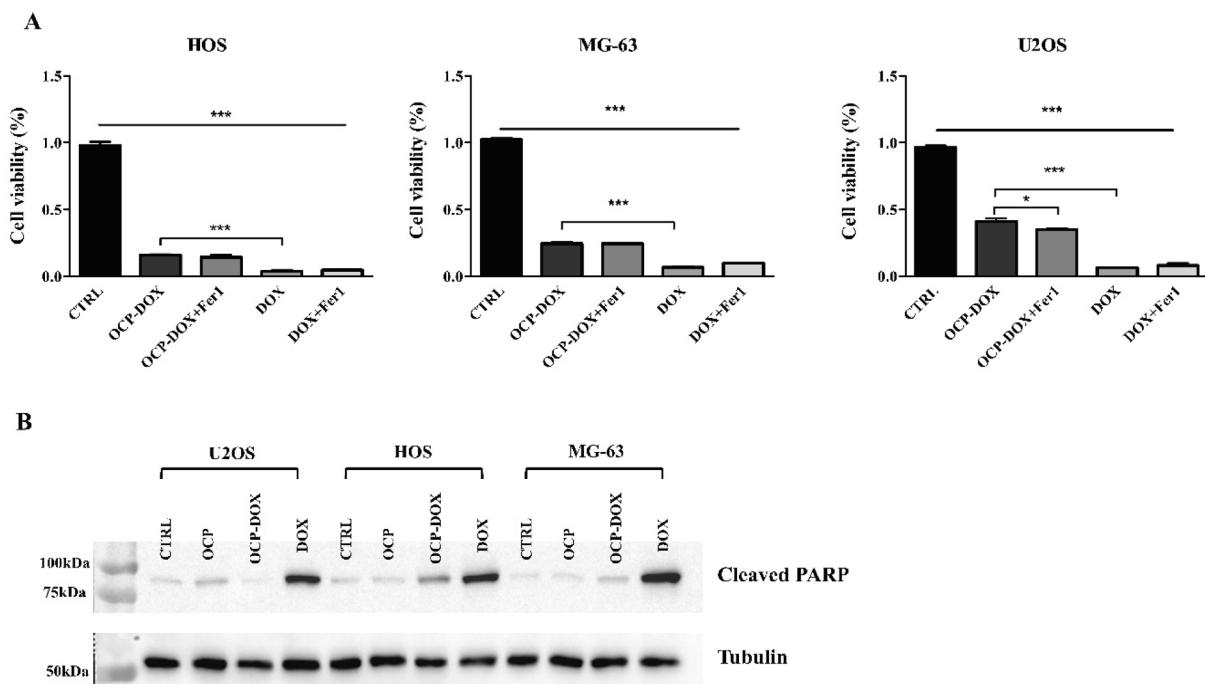


Fig. 8. Characterization of cell death induced by DOX-loaded OCP powder in osteosarcoma cells. (A) U2OS, HOS, and MG63 cells were exposed for 72 h to 1DOX-OCP, pure OCP or doxorubicin alone or in combination with 10 μ M of Fer1 (OCP-DOX + Fer1, DOX + Fer1) and cell viability was evaluated in AlamarBlue-stained cells. (B) Protein levels of cleaved PARP were evaluated in osteosarcoma cells exposed as in (A), by western blotting analysis. GAPDH was used as a loading control. Histograms represent mean \pm s.d.; n = 3; *p < 0.05, ***p < 0.001.

characterized as an initial burst release of DOX (Fig. 4A) and 2) the drug was also incorporated inside the OCP's water layer (seen through the shifts of characteristic OCP peaks in XRD, Fig. 1 A,B) that helped with the prolonged drug release as the OCP construct slowly transformed to a more stable phase. As a corroboration that the release was slower if the drug loading was done at the same time as the OCP was forming (*in situ* method), the adsorption experiment was also performed, DOX release was tested for 48 h and obtained results clearly evidenced that the initial burst release in this case is drastically higher (up to 50 % compared to *in situ*) and no changes in the crystal structure of OCP were noticed. Due to the other advantages of this methodology, for instance, low cost, facile preparation method, presence of a single precursor and the environmentally friendly approach, DOX-OCP application in drug delivery has shown high potential.

The *in vitro* cell studies exhibited time and concentration-dependent decrease in the proliferation rate of MG63 and MC3T3 cells, when they were exposed to the DOX-loaded OCP powders. Complex formulation between DOX and CaP in the proposed DDS potentially enhances the cytotoxic properties of the drug, as seen in previous studies. This additional effect of complexation could contribute to increased cytotoxicity against cancer cells. However, the potential of OCP powders to enhance cell proliferation through the presence of elevated Ca^{2+} ions in the surrounding medium has also been recorded throughout different studies. This additional data demonstrated that the interaction between calcium and doxorubicin, instead of a synergistic effect, reduced the efficacy of doxorubicin and led to a recovery in cell viability. Once the pathway of programmed cell death responsible for the aforementioned cytotoxic effect was tested, it showed that apoptosis is the main pathway.

As the DOX-OCP drug delivery system would be administered locally in the cancer site, aside of the therapeutic effect the drug would offer, OCP could have an ameliorating outcome on the bone regeneration process. DOX-OCP application would potentially be interchangeable and could range from the composite scaffolds or protective coatings (e.g., with alginate) to injectable bone cements and even the granular shape of the powders themselves. However, even if the DOX-OCP drug delivery system has already shown a prolonged drug release in PBS (7.4 and 6.0 pH), additional improvements in terms of the *in vitro* drug release and the control of the initial burst release (e.g., addition of the polymer) are still needed. Thus, testing of such advanced constructs, followed by a wider scope of *in vitro* conditions, as well as additional biological tests, will be worth investigating in future studies.

5. Data availability statement

The datasets used and/or analysed during the current study are available from the corresponding author on reasonable request.

CRediT authorship contribution statement

Ilijana Kovrlija: Writing – review & editing, Writing – original draft, Visualization, Investigation, Formal analysis, Conceptualization. **Elżbieta Pańczyszyn:** Writing – original draft, Investigation, Formal analysis. **Oznur Demir:** Writing – review & editing, Writing – original draft, Investigation, Formal analysis. **Marta Laizane:** Formal analysis. **Marco Corazzari:** Supervision. **Janis Locs:** Writing – review & editing, Resources, Funding acquisition, Conceptualization. **Dagnija Loca:** Writing – review & editing, Supervision, Resources, Funding acquisition, Conceptualization.

Declaration of competing interest

The authors declare that they have no known competing financial interests or personal relationships that could have appeared to influence the work reported in this paper.

Data availability

Data will be made available on request.

Acknowledgement

The authors acknowledge the financial support for granting Open Access and access to the infrastructure and expertise from the European Union's Horizon 2020 Research and Innovation programme under grant agreement [No. 857287 (BBCE)], as well as the European Union's Horizon 2020 Research and Innovation programme under the Marie Skłodowska-Curie grant agreement [No. 860462 (PREMUROSA)].

Appendix A. Supplementary data

Supplementary data to this article can be found online at <https://doi.org/10.1016/j.ijpharm.2024.123932>.

References

- Akutsu, M., Kano, Y., Tsunoda, S., Suzuki, K., Yazawa, Y., Miura, Y., 1995. Schedule-dependent interaction between paclitaxel and doxorubicin in human cancer cell lines *in vitro*. *European Journal of Cancer* 31 (13–14), 2341–2346. [https://doi.org/10.1016/0959-8049\(95\)00448-3](https://doi.org/10.1016/0959-8049(95)00448-3).
- Anada, T., Araseki, A., Matsukawa, S., Yamasaki, T., Kamakura, S., & Suzuki, O. (2008). Effect of octacalcium phosphate ionic dissolution products on osteoblastic cell differentiation. *Key Engineering Materials*, 361–363 I, 31–34. Doi: 10.4028/www.scientific.net/kem.361-363.31.
- Banerjee, D., Bose, S., 2019. Comparative effects of controlled release of sodium bicarbonate and doxorubicin on osteoblast and osteosarcoma cell viability. *Materials Today Chemistry* 12, 200–208. <https://doi.org/10.1016/j.mtchem.2018.11.008>.
- Bordbar-Khiabani, A., Kovrlija, I., Locs, J., Loca, D., Gasik, M., 2023. Octacalcium Phosphate-Laden Hydrogels on 3D-Printed Titanium Biomaterials Improve Corrosion Resistance in Simulated Biological Media. *International Journal of Molecular Sciences* 24 (17). <https://doi.org/10.3390/ijms241713135>.
- Chaitanya, G.V., Alexander, J.S., Babu, P.P., 2010. PARP-1 cleavage fragments: Signatures of cell-death proteases in neurodegeneration. *Cell Communication and Signaling* 8, 1–11. <https://doi.org/10.1186/1478-811X-8-31>.
- Chen, X., Comish, P.B., Tang, D., Kang, R., 2021. Characteristics and Biomarkers of Ferroptosis. *Frontiers in Cell and Developmental Biology* 9 (January), 1–9. <https://doi.org/10.3389/fcell.2021.637162>.
- Chow, L.C., Eanes, E.D., 2001. Octacalcium phosphate. In: *Monographs in Oral Science* Vol. 18. <https://doi.org/10.1007/springerreference.39293>.
- Cree, I.A., Charlton, P., 2017. Molecular chess? Hallmarks of anti-cancer drug resistance. *BMC Cancer* 1–8. <https://doi.org/10.1186/s12885-016-2999-1>.
- Demir, O., Pylostomou, A., Loca, D., 2023. Octacalcium phosphate phase forming cements as an injectable bone substitute materials: Preparation and *in vitro* structural study. *Biomaterials Advances* 107386. <https://doi.org/10.1016/j.bioadv.2023.213731>.
- Dorozhkin, S.V., 2016. Multiphasic calcium orthophosphate (CaPO₄) bioceramics and their biomedical applications. *Ceramics International* 42 (6), 6529–6554. <https://doi.org/10.1016/j.ceramint.2016.01.062>.
- Elbayoumi, T.A., Torchilin, V.P., 2009. Tumor-targeted nanomedicines: Enhanced antitumor efficacy *in vivo* of doxorubicin-loaded, long-circulating liposomes modified with cancer-specific monoclonal antibody. *Clinical Cancer Research* 15 (6), 1973–1980. <https://doi.org/10.1158/1078-0432.CCR-08-2392>.
- Fu, J., Li, T., Yang, Y., Jiang, L., Wang, W., Fu, L., Zhu, Y., Hao, Y., 2021. Activatable nanomedicine for overcoming hypoxia-induced resistance to chemotherapy and inhibiting tumor growth by inducing collaborative apoptosis and ferroptosis in solid tumors. *Biomaterials* 268, 120537. <https://doi.org/10.1016/j.biomaterials.2020.120537>.
- Gagliardi, M., Saverio, V., Rossin, F., D'Eletto, M., Corazzari, M., 2023. Transglutaminase 2 and Ferroptosis: a new liaison? *Cell Death Discovery* 9 (1), 7–9. <https://doi.org/10.1038/s41420-023-01394-1>.
- Gautier, J., Munnier, E., Paillard, A., Hervé, K., Douziech-Eyrolles, L., Soucé, M., Dubois, P., Chourpa, I., 2012. A pharmaceutical study of doxorubicin-loaded PEGylated nanoparticles for magnetic drug targeting. *International Journal of Pharmaceutics* 423 (1), 16–25. <https://doi.org/10.1016/j.ijpharm.2011.06.010>.
- Génin, F.Y., Luo, P., Dash, K., 2004. Hydroxyapatite based drug delivery implant for cancer treatment. *United States Patent* 1 (12).
- Guise, T.A., 2006. Bone Loss and Fracture Risk Associated with Cancer Therapy. *The Oncologist* 11 (10), 1121–1131. <https://doi.org/10.1634/theoncologist.11-10-1121>.
- Honda, Y., Kamakura, S., Sasaki, K., Suzuki, O., 2007. Formation of bone-like apatite enhanced by hydrolysis of octacalcium phosphate crystals deposited in collagen matrix. *Journal of Biomedical Materials Research - Part B Applied Biomaterials* 80 (2), 281–289. <https://doi.org/10.1002/jbm.b.30595>.
- Iafisco, M., Drouet, C., Adamiano, A., Pascaud, P., Montesi, M., Panseri, S., Sarda, S., Tampieri, A., 2016. Superparamagnetic iron-doped nanocrystalline apatite as a delivery system for doxorubicin. *J. Mater. Chem. B* 4, 57–70. <https://doi.org/10.1039/c5tb01524c>.

- Ito, N., Kamitakahara, M., Ioku, K., 2014. Preparation and evaluation of spherical porous granules of octacalcium phosphate/hydroxyapatite as drug carriers in bone cancer treatment. *Materials Letters* 120, 94–96. <https://doi.org/10.1016/j.matlet.2014.01.040>.
- Jablonska-Trypuc, A., Swiderski, G., Kretowski, R., Lewandowski, W., 2017. Newly Synthesized Doxorubicin Complexes with Selected Metals — Synthesis, Structure and Anti-Breast Cancer Activity. *Molecules* 22, 1106. <https://doi.org/10.3390/molecules22071106>.
- Ji, P., Yu, L., Guo, W.C., Mei, H.J., Wang, X.J., Chen, H., Fang, S., Yang, J., 2015. Doxorubicin inhibits proliferation of osteosarcoma cells through upregulation of the Notch signaling pathway. *Oncology Research* 22 (4), 185–191. <https://doi.org/10.3727/096504015X14343704124340>.
- Jiang, Xiaodan, Zhao, Y., Wang, C., Sun, R., & Tang, Y. (2022). Effects of physico-chemical properties of ions-doped hydroxyapatite on adsorption and release performance of doxorubicin as a model anticancer drug. *Materials Chemistry and Physics*, 276(August 2021), 125440. Doi: 10.1016/j.matchemphys.2021.125440.
- Jiang, X., Stockwell, B.R., Conrad, M., 2021. Ferroptosis: mechanisms, biology and role in disease. *Nature Reviews Molecular Cell Biology* 22 (4), 266–282. <https://doi.org/10.1038/s41580-020-00324-8>.
- Kovrljica, I., Locs, J., Loca, D., 2021. Octacalcium phosphate: Innovative vehicle for the local biologically active substance delivery in bone regeneration. *Acta Biomaterialia* 135, 27–47. <https://doi.org/10.1016/j.actbio.2021.08.021>.
- Kovrljica, I., Menshikh, K., Marsan, O., Rey, C., Combes, C., Locs, J., Loca, D., 2023. Exploring the Formation Kinetics of Octacalcium Phosphate from Alpha-Tricalcium Phosphate : Synthesis Scale-Up, Determination of Transient Phases. Their Morphology and Biocompatibility. *Biomolecules*, p. 13.
- Lebugle, A., Rodrigues, A., Bonnevalle, P., Voigt, J.J., Canal, P., Rodriguez, F., 2002. Study of implantable calcium phosphate systems for the slow release of methotrexate. *Biomaterials* 23, 3517–3522.
- LeGeros, R.Z., Daculsi, G., Orly, I., Abergas, T., Torres, W., 1989. Solution-mediated formation of octacalcium phosphate (OCP) to apatite. *Scanning Microscopy* 3 (1), 129–138.
- Li, J., Yang, Z., Li, Y., Xia, J., Li, D., Li, H., Ren, M., Liao, Y., Yu, S., Chen, Y., Yang, Y., Zhang, Y., 2016. Cell apoptosis, autophagy and necroptosis in osteosarcoma treatment. *Oncotarget* 7 (28), 44763–44778. <https://doi.org/10.18632/oncotarget.8206>.
- Li, S., Zhang, H., Liu, J., Shang, G., 2023. Targeted therapy for osteosarcoma: a review. *Journal of Cancer Research and Clinical Oncology* 149 (9), 6785–6797. <https://doi.org/10.1007/s00432-023-04614-4>.
- Lin, R., Shi, L., Wang, C., 2005. In vitro study of anticancer drug doxorubicin in PLGA-based microparticles. *Biomaterials* 26, 4476–4485. <https://doi.org/10.1016/j.biomaterials.2004.11.014>.
- Liu, X., Du, S., Wang, S., Ye, K., 2022a. Ferroptosis in osteosarcoma: A promising future. *Frontiers in Oncology* 12 (November), 1–9. <https://doi.org/10.3389/fonc.2022.1031779>.
- Liu, Y., Raina, D.B., Sebastian, S., Nagesh, H., Isaksson, H., Engellau, J., Lidgren, L., Tägil, M., 2021. Sustained and controlled delivery of doxorubicin from an in-situ setting biphasic hydroxyapatite carrier for local treatment of a highly proliferative human osteosarcoma. *Acta Biomaterialia* 131, 555–571. <https://doi.org/10.1016/j.actbio.2021.07.016>.
- Liu, Y., Nadeem, A., Sebastian, S., Olsson, M.A., Wai, S.N., Lidgren, L., Styring, E., Engellau, J., Isaksson, H., Magnus, T., Raina, D.B., 2022b. Bone mineral: A trojan horse for bone cancers. Efficient mitochondria targeted delivery and tumor eradication with nano hydroxyapatite containing doxorubicin. *Materials Today Bio* 14 (December 2021). <https://doi.org/10.1016/j.mtbio.2022.100227>.
- Loca, D., Sokolova, M., Locs, J., Smirnova, A., Irbe, Z., 2015. Calcium phosphate bone cements for local vancomycin delivery. *Materials Science and Engineering C* 49 (1), 106–113. <https://doi.org/10.1016/j.msec.2014.12.075>.
- Martinez, T., Sarda, S., Dupret-Bories, A., Charvillat, C., Projetti, F., Drouet, C., 2021. Toward a doxorubicin-loaded bioinspired bone cement for the localized treatment of osteosarcoma. *Future Oncology* 17 (26), 3511–3528. <https://doi.org/10.2217/fon-2021-0128>.
- Mathew, M., Brown, W.E., Schroeder, L.W., Dickens, B., 1988. Crystal structure of octacalcium bis(hydrogenphosphate) tetrakis(phosphate)pentahydrate, Ca₈(HP0₄)₂(PO₄)₄·5H₂O. *Journal of Crystallographic and Spectroscopic Research* 18 (3), 235–250. <https://doi.org/10.1007/BF01194315>.
- Miotto, G., Rossetto, M., Di Paolo, M.L., Orian, L., Venerando, R., Roveri, A., Vučković, A. M., Bosello Travain, V., Zaccarin, M., Zennaro, L., Maiorino, M., Toppo, S., Ursini, F., Cozza, G., 2020. Insight into the mechanism of ferroptosis inhibition by ferrostatin-1. *Redox Biology* 28 (September 2019), 101328. <https://doi.org/10.1016/j.redox.2019.101328>.
- Modh, H., Fang, D.J., Ou, Y.H., Yau, J.N.N., Kovshova, T., Nagpal, S., Knoll, J., Wallenwein, C.M., Maiti, K., Bhowmick, S., Gelperina, S., Pastorin, G., Wacker, M.G., 2021. Injectable drug delivery systems of doxorubicin revisited: In vitro-in vivo relationships using human clinical data. *International Journal of Pharmaceutics* 608 (April), 121073. <https://doi.org/10.1016/j.ijpharm.2021.121073>.
- Mosina, M., Kovrljica, I., Stipniece, L., Locs, J., 2022. Gallium containing calcium phosphates: Potential antibacterial agents or fictitious truth. *Acta Biomaterialia* 150, 48–57. <https://doi.org/10.1016/j.actbio.2022.07.063>.
- Nussinov, R., Tsai, C., Jang, H., 2021. Anticancer drug resistance : An update and perspective. *Drug Resistance Updates* 59, 100796. <https://doi.org/10.1016/j.drug.2021.100796>.
- Olson, R.D., Mushlin, P.S., 1990. Doxorubicin cardiotoxicity: analysis of prevailing hypotheses. *The FASEB Journal* 4.
- Parent, M., Baradari, H., Champion, E., Damia, C., Viana-trecant, M., 2017. Design of calcium phosphate ceramics for drug delivery applications in bone diseases : A review of the parameters affecting the loading and release of the therapeutic substance. *Journal of Controlled Release* 252, 1–17. <https://doi.org/10.1016/j.jconrel.2017.02.012>.
- Pelss, J., Loca, D., Berzina-Cimdina, L., Locs, J., Lakevics, V., 2011. Release of anticancer drug doxorubicin from biodegradable polymer coated porous hydroxyapatite scaffolds. *Advanced Materials Research* 284–286, 1770–1773. <https://doi.org/10.4028/www.scientific.net/AMR.284-286.1770>.
- Pfeffer, C.M., Singh, A.T.K., 2018. Apoptosis: A target for anticancer therapy. *International Journal of Molecular Sciences* 19 (2). <https://doi.org/10.3390/ijms19020448>.
- Pinski, J., Parikh, A., Bova, G.S., Isaacs, J.T., 2001. Therapeutic Implications of Enhanced G0/G1 Checkpoint Control Induced by Coculture of Prostate Cancer Cells with Osteoblasts. *Cancer Research* 61 (9), 6372–6376.
- Pisa, R., Kapoor, T.M., 2020. Chemical strategies to overcome resistance against targeted anticancer therapeutics. *Nature Chemical Biology* 16 (August), 817–825. <https://doi.org/10.1038/s41589-020-0596-8>.
- Pylostomou, A., Oznur, D., Loca, D., 2023. Calcium phosphate bone cements as local drug delivery systems for bone cancer treatment. *Biomaterials*. *Advances* 148 (February). <https://doi.org/10.1016/j.bioadv.2023.213367>.
- Qi, C., Zhu, Y.J., Sun, T.W., Wu, J., Chen, F., 2015. Microwave-Assisted Hydrothermal Rapid Synthesis of Amorphous Calcium Phosphate Mesoporous Microspheres Using Adenosine 5'-Diphosphate and Application in pH-Responsive Drug Delivery. *Chemistry - An Asian Journal* 10 (11), 2503–2511. <https://doi.org/10.1002/asia.201500667>.
- Qiu, C., Liu, T., Luo, D., Luan, D., Cheng, L., Wang, S., 2022. Novel Therapeutic Savior for Osteosarcoma: The Endorsement of Ferroptosis. *Frontiers in Oncology* 12 (March), 1–7. <https://doi.org/10.3389/fonc.2022.746030>.
- Roncuzzi, L., Pancotti, F., Baldini, N., 2014. Involvement of HIF-1 α activation in the doxorubicin resistance of human osteosarcoma cells. *Oncology Reports* 32 (1), 389–394. <https://doi.org/10.3892/or.2014.3181>.
- Saito, S., Hamai, R., Shiwaku, Y., Hasegawa, T., Sakai, S., Tsuchiya, K., Sai, Y., Iwama, R., Amizuka, N., Takahashi, T., Suzuki, O., 2021. Involvement of distant octacalcium phosphate scaffolds in enhancing early differentiation of osteocytes during bone regeneration. *Acta Biomaterialia* 129, 309–322. <https://doi.org/10.1016/j.actbio.2021.05.017>.
- Shi, H., Yang, S., Zeng, S., Liu, X., Zhang, J., Zhang, J., Wu, T., Ye, X., Yu, T., Zhou, C., Ye, J., 2019. Enhanced angiogenesis of biodegradable iron-doped octacalcium phosphate/poly (lactic-co-glycolic acid) scaffold for potential cancerous bone regeneration. *Applied Materials Today* 15, 100–114. <https://doi.org/10.1016/j.apmt.2019.01.002>.
- Siebler, T., Shalet, S.M., Robson, H., 2002. Effects of chemotherapy on bone metabolism and skeletal growth. *Hormone Research* 58 (SUPPL. 1), 80–85. <https://doi.org/10.1159/000064769>.
- Singh, V., Khurana, A., Navik, U., Allawadhi, P., Bharani, K.K., Weiskirchen, R., 2022. Apoptosis and Pharmacological Therapies for Targeting Thereof for Cancer Therapeutics. *Sci* 4 (2). <https://doi.org/10.3390/sci4020015>.
- Sritharan, S., Sivalingam, N., 2021. A comprehensive review on time-tested anticancer drug doxorubicin. *Life Sciences* 278, 119527. <https://doi.org/10.1016/j.lfs.2021.119527>.
- Suzuki, O., Inslay, G., 2020. Octacalcium Phosphate Biomaterials. *Woodhead Publishing Series in Biomaterials*.
- Tacar, O., Sriamornsak, P., Dass, C.R., 2012. Doxorubicin: an update on anticancer molecular action, toxicity and novel drug delivery systems. *Journal of Pharmacy and Pharmacology* 65, 157–170. <https://doi.org/10.1111/j.2042-7158.2012.01567.x>.
- Tang, Q., Zhu, Y., Wu, J., Chen, F., Cao, S.-W., 2011. Calcium phosphate drug nanocarriers with ultrahigh and adjustable drug-loading capacity: One-step synthesis, in situ drug loading and prolonged drug release. *Nanomedicine: Nanotechnology, Biology, and Medicine* 7 (4), 428–434. <https://doi.org/10.1016/j.nano.2010.12.005>.
- Tani, T., Okada, K., Takahashi, S., Suzuki, N., Shimada, Y., Itoi, E., 2006. Doxorubicin-loaded Calcium Phosphate Cement in the Management of Bone and Soft Tissue Tumors. *In Vivo* 60, 55–60.
- Thorn, C.F., Oshiro, C., Marsh, S., Hernandez-Boussard, T., McLeod, H., Klein, T.E., Altman, R.B., 2011. Doxorubicin pathways: Pharmacodynamics and adverse effects. *Pharmacogenetics and Genomics* 21 (7), 440–446. <https://doi.org/10.1097/FPC.0b013e32833ff566>.
- Thuy, T., Nguyen, T., Lim, Y.J., Hui, M., Fan, M., Jackson, R.A., Lim, K.K., Ang, W.H., Hon, K., Ban, K., Chen, E.S., 2016. Calcium modulation of doxorubicin cytotoxicity in yeast and human cells. *Genes to Cells* 226–240. <https://doi.org/10.1111/gtc.12346>.
- van der Zanden, S.Y., Qiao, X., Neeffes, J., 2021. New insights into the activities and toxicities of the old anticancer drug doxorubicin. *The FEBS Journal* 288, 6095–6111. <https://doi.org/10.1111/febs.15583>.
- Wang, J., de Boer, J., de Groot, K., 2009. Proliferation and differentiation of osteoblast-like MC3T3-E1 cells on biomimetically and electrolytically deposited calcium phosphate coatings. *Journal of Biomedical Materials Research. Part A* 90 (3), 664–670. <https://doi.org/10.1002/jbm.a.32128>.
- Wang, X., Hua, P., He, C., Chen, M., 2022. Non-apoptotic cell death-based cancer therapy: Molecular mechanism, pharmacological modulators, and nanomedicine. *Acta Pharmaceutica Sinica B* 12 (9), 3567–3593. <https://doi.org/10.1016/j.apsb.2022.03.020>.
- Wang, S., Konorev, E.A., Kotamraju, S., Joseph, J., Kalivendi, S., Kalyanaraman, B., 2004. Doxorubicin induces apoptosis in normal and tumor cells via distinctly different mechanisms: Intermediacy of H2O2- and p53-dependent pathways. *Journal of Biological Chemistry* 279 (24), 25535–25543. <https://doi.org/10.1074/jbc.M400944200>.

- Wang, A.Z., Langer, R., Farokhzad, O.C., 2012. Nanoparticle delivery of cancer drugs. *Annual Review of Medicine* 63, 185–198. <https://doi.org/10.1146/annurev-med-040210-162544>.
- Wen, S.h., Su, S.C., Liou, B.H., Lin, C.H., Lee, K.R., 2018. Sulbactam-enhanced cytotoxicity of doxorubicin in breast cancer cells. *Cancer Cell International* 18 (1), 1–18. <https://doi.org/10.1186/s12935-018-0625-9>.
- Wilson, B.E., Jacob, S., Yap, M.L., Ferlay, J., Bray, F., Barton, M.B., 2019. Estimates of global chemotherapy demands and corresponding physician workforce requirements for 2018 and 2040: a population-based study. *Lancet Oncology* 20 (6), 769–780. [https://doi.org/10.1016/S1470-2045\(19\)30163-9](https://doi.org/10.1016/S1470-2045(19)30163-9).
- Yang, X., Gao, X., Gan, Y., Gao, C., Zhang, X., Ting, K., Wu, B.M., Gou, Z., 2010. Facile synthesis of octacalcium phosphate nanobelts: Growth mechanism and surface adsorption properties. *Journal of Physical Chemistry C* 114 (14), 6265–6271. <https://doi.org/10.1021/jp911576f>.
- Yao, Z., Murali, B., Ren, Q., Luo, X., Faget, D.V., Cole, T., Ricci, B., Thotala, D., Monahan, J., Van Deursen, J.M., Baker, D., Faccio, R., Schwarz, J.K., Stewart, S.A., 2020. Therapy-induced senescence drives bone loss. *Cancer Research* 80 (5), 1171–1182. <https://doi.org/10.1158/0008-5472.CAN-19-2348>.
- Yin, J., Guo, J., Zhang, Q., Cui, L., Zhang, L., Zhang, T., Zhao, J., Li, J., Middleton, A., Carmichael, P.L., Peng, S., 2018. Toxicology in Vitro Doxorubicin-induced mitophagy and mitochondrial damage is associated with dysregulation of the PINK1 / parkin pathway. *Toxicology in Vitro* 51 (April), 1–10. <https://doi.org/10.1016/j.tiv.2018.05.001>.